# ELEMENTAL ANALYSIS

# BY

# NEUTRON TIME-OF-FLIGHT SPECTROMETRY



by

P.J. Strebel

Supervisors: Prof. E.C. Leisegang

Dr. M. Peisach

A thesis submitted in partial
fulfilment of the requirements
for the degree of Master of Science
at the University of Cape Town.

September, 1967.

ACKNOWLEDGEMENTS

The author is greatly indebted to:

Dr. M. Peisach for suggesting the investigation, for his help and guidance during its course, and for his continuous encouragement in the form of many stimulating discussions.

Prof. E.C. Leisegang for promoting the investigation.

Mr. R. Pretorius for his advice and assistance during irradiations.

Dr. J.J. Kritzinger for his assistance in the design of the new irradiation cell and Messrs. T. Swart and T. Beck for constructing the irradiation cells.

The Council for Scientific and Industrial Research for the bursary which made the work possible.

The Southern Universities Nuclear Institute for the facilities that were made available and members of the staff for their co-operation.

Mr. H. Schmitt for his aid with the drawings.

Miss H. Luitingh for typing the script.

C O N T E N T S

# C H A P T E R  I

## INTRODUCTION

# ACTIVATION ANALYSIS

Activation analysis can be described as an elemental or isotopic analysis based on the detection and measurement of characteristic radioactivity produced by selected nuclear reactions. The method owes its origin to the discovery of induced or artificial radioactivity by Curie and Joliot in 1933 (1). The potential value of this discovery for the solution of analytical problems was soon recognized and demonstrated by Hevesy and Levi (2), who in 1936 used thermal neutrons to determine the concentration of dysprosium in impure yttrium. In 1938 Seaborg and Livingood (3) applied deuteron beams to the determination of trace quantities of gallium in high purity iron. Since then, activation analysis has established itself as a powerful tool for the determination of a wide range of elements, and it has been applied to such diverse fields as archeology, analytical chemistry, biological and medical research, geochemistry, nuclear reactor technology, and to the measurement of physical properties of materials, such as vapour pressure, particle size and homogeneity. The method owes its success to the sensitivity with which small amounts of radioactive material can be measured and the availability of high neutron and charged particle fluxes brought about by the development of nuclear reactors and particle accelerators.

In general a nuclear reaction may be written as

$$X(x,y)Y \quad \ldots\ldots\ldots\ldots\ldots\ldots\ldots\ldots\ldots\ldots \quad (1)$$

which indicates that nuclei, X, on being bombarded with

particles or energy quanta, x, promptly emit one or more particles, y, to form product nuclei, Y. When the product nucleus, Y, is radioactive the measurement of its activity can be used to determine the nuclide, X. This is the fundamental feature of activation analysis. The activity, A, in disintegrations per sec., produced in n target nuclei, irradiated for a time t, in a constant flux of $\phi$ particles per $cm.^2$ per sec. by a reaction with cross section $\sigma$ (which is a measure of the reaction probability), is given by

$$A = n.\sigma.\phi.(1-e^{-0.693t/\tau}) \quad \ldots\ldots\ldots\ldots\ldots\ldots \quad (2)$$

where $\tau$ is the half-life of the radioactive product, Y.

Despite its wide range of application the method of activation analysis becomes impractical if:

(i) the half-life of Y is very short, because special methods of fast transfer to the counting apparatus become necessary.

(ii) the half-life of Y is very long, because the irradiation time required to produce sufficient activity will be prohibitive unless the cross section for the reaction is large (see equation 2).

(iii) Y emits low energy radiation, because the detection sensitivity may often be poor.

Moreover, the method of activation analysis fails entirely in the following cases:

(i) when the sample under investigation contains other elements which yield the same radioactive product, Y.

(ii) when interfering radioactive products cannot be separated and their radiation cannot be distinguished from that of Y.

(iii) when Y is stable.

## ANALYSIS USING PROMPT EMISSION

Some of the shortcomings of activation analysis may be circumvented by counting the prompt particles, y, emitted during the nuclear reaction. The energies of such particles may be used to identify the original target nuclide, X, and the number of particles to provide a quantitative estimate of X. The cross section, $\sigma$, of a nuclear reaction is a function of the energy of the bombarding particle beam, $E_i$, and the angle, $\theta$, at which the product particles are detected, relative to the direction of incidence of the bombarding beam. The number of prompt particles, N, detected per sec. from a nuclear reaction is given by

$$N = n.\phi.\varepsilon.\Omega.\sigma(E_i,\theta) \quad \ldots\ldots\ldots\ldots\ldots\ldots \quad (3)$$

where n is the number of target nuclei in the path of the beam, $\phi$ is the flux of the beam in particles per $cm.^2$ per sec., $\varepsilon$ is the efficiency of the measuring system and $\Omega$ is the solid angle subtended by the measuring system at the target.

The measurement of prompt reaction products greatly

increases the scope of nuclear methods of elemental and isotopic analysis. It makes such methods independent of the radioactive decay properties of the product nucleus, Y. Furthermore, the rate of accumulation of data remains constant with time and does not decrease as is the case with radioactive material. At the end of the irradiation all the information has been obtained and subsequent counting periods, as are necessary for radioactive material, become meaningless.

The potential analytical use of prompt particles emitted during a nuclear reaction will depend on the nature of the particles, and, in particular, the ease with which the particles can be measured. Reaction products which have high penetrating powers such as neutrons or gamma-rays will *a priori* offer greater scope than charged particles such as protons, deuterons or alpha-particles which may be stopped within the target mass. Although extensive measurements have been made of the prompt gamma-rays emitted during neutron capture reactions, the measurement of prompt neutrons has hardly been investigated. This is surprising because neutrons may readily be detected against a background of other radiation.

Prompt neutrons were first used for analytical purposes by Butler (4), who determined deuterium in alloys by using a beam of deuterons and counting the total number of neutrons produced by the reaction $^{2}H(d,n)^{3}He$. However, the total neutron count did not discriminate against neutrons from other sources and Butler reported interference from oxygen when the

threshold for the reaction $^{16}O(d,n)^{17}F$ was exceeded. Interfering neutrons, which further reduced the sensitivity of the method, were also produced by (d,n) reactions on the aluminium beam tubes and on the nitrogen-14 in the residual air in the vacuum system.

The disadvantage of gross neutron counting lies in the fact that all the neutrons are counted without reference to their source of origin but this disadvantage can be overcome if the energy of the neutron is measured. Hence, any experimental method capable of differentiating between the various neutron energies could serve as the basis of an analytical procedure whereby the number of neutrons of a fixed energy could be used as a measure of the content of the target nuclide in the sample under investigation.

## NEUTRON TIME-OF-FLIGHT SPECTROMETRY

The energy of a neutron, $\underline{E}_n$, emitted from a nuclear reaction is determined by the $\underline{Q}$-value of the reaction, the energy of the particle incident on the nucleus, $\underline{E}_i$, and the angle $\theta$ at which it is emitted. From the kinematics of a nuclear reaction (5) the energy of the neutron is given by

$$\sqrt{E_n} = v \pm \sqrt{v^2 + w} \quad \ldots\ldots\ldots\ldots\ldots\ldots\ldots \quad (4)$$

where

$$v \equiv \frac{\sqrt{m_i m_n E_i}}{(m_n + M)} \text{Cos}\theta$$

and

$$w \equiv \frac{MQ + E_i(M - m_i)}{(m_n + M)} .$$

$\underline{m}_i$, $\underline{m}_n$ and $\underline{M}$ refer to the masses of the incident particle, the neutron and the product nucleus respectively. The energy relationship expressed quantitatively in equation 4 may be represented diagrammatically as in Figure 1. It is clear that the neutrons resulting from a particular reaction will have discrete energies related to the $\underline{Q}$-values corresponding to the various excited states in which the product nucleus is left.

The most accurate method available at present for neutron spectrometry is the time-of-flight technique in which the time, $\underline{t}$, taken by a neutron to cover a distance, $\underline{d}$, is measured and related non-relativistically to the energy of the neutron by

$$t = \frac{72.3 \times d}{\sqrt{E_n}} \quad \ldots\ldots\ldots\ldots\ldots\ldots\ldots\ldots \quad (5)$$

where the constant includes the mass of the neutron and the relevant conversion units if $\underline{t}$ is measured in nsec., $\underline{d}$ in metres and $\underline{E}_n$ in MeV. The energy resolution of a time-of-flight spectrometer is given (6) by

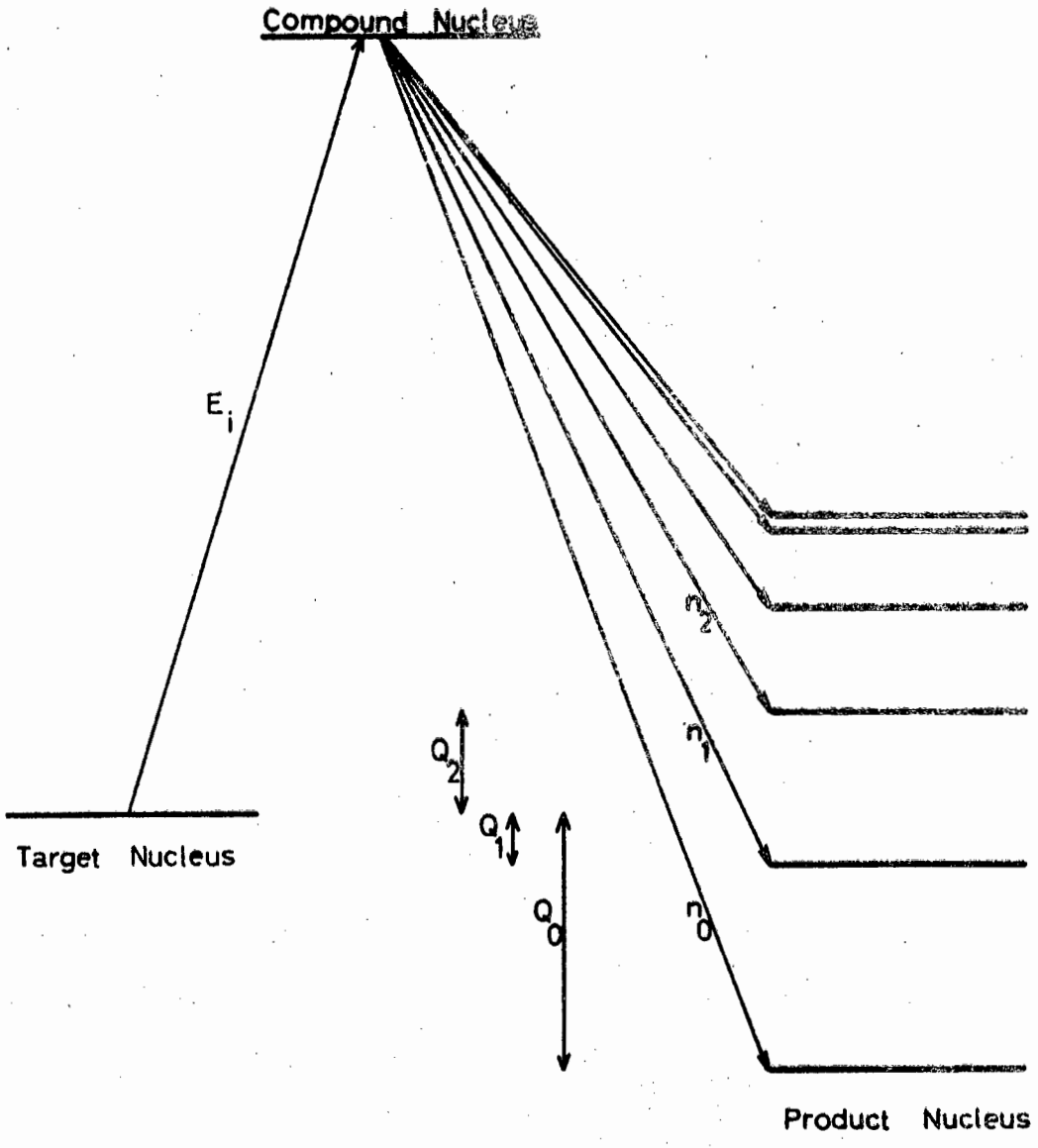


FIGURE 1. SCHEMATIC REPRESENTATION OF PROMPT NEUTRON EMISSION

$$\frac{\Delta E_n}{E_n} = \left[\left(\frac{\Delta t . E_n}{36 . d}\right)^2 + \left(\frac{2 . \Delta d}{d}\right)^2\right]^{1/2} \quad \ldots\ldots\ldots \quad (6)$$

where $\Delta E_n$ is the neutron energy uncertainty (in MeV), $\Delta t$ is the timing uncertainty (in nsec.) and $\Delta d$ is the flight path uncertainty (in metres).

When the irradiating beam consists of pulses of short duration separated by a time interval of sufficient length, it is possible to use the arrival of the pulse at the target as the instant of neutron generation and the arrival of the neutron at the detector to mark the end of the time-of-flight. Recent developments in electronics have made it possible to measure such short time intervals, thus making neutron time-of-flight spectrometry practicable.

The use of neutron time-of-flight spectrometry for analysis was first suggested by Peisach and Pretorius (7,8), and has already been used for solid samples (9,10) and for gases (11) which do not decompose at high temperatures.

## OBJECTIVES OF THIS INVESTIGATION

Among the more common elements for which neutron activation analysis is not sufficiently sensitive, are carbon, nitrogen and oxygen. These elements are so important that they were selected for study in an attempt to extend the advantages

of nuclear methods of analysis to their determination.

The physical state of a sample submitted to activation analysis frequently determines whether activation analysis is possible or not. Although most solids can readily be submitted to activation analysis, the same does not apply to liquids or gases. In the case of liquids, their radiolytic decomposition may yield gaseous products which could endanger the irradiation facility whilst gases, with few exceptions, present serious technical difficulties for irradiation with reactor neutrons. Clearly the development of a method suitable for the analysis of gases would serve a useful purpose.

When carbon, nitrogen and oxygen are irradiated with a pulsed deuteron beam (d,n) reactions can occur and their Q-values are given in Table I. From equation 4 and the Q-values listed in Table I, the energies of neutrons measured at $30^{o}$ and generated by a deuteron beam of 3 MeV have been calculated and are given in the same table. From these values it is clear that the neutron energies are sufficiently different to enable them to be used for spectrometry. For a particular nuclear reaction and at a selected deuteron energy, the number of neutrons emitted of any particular energy will depend on the number of target nuclei in the path of the beam; in the case of gases, the number of neutrons emitted per unit beam current at a fixed angle will be directly proportional to the pressure of the gas, provided the volume of the gas irradiated remains constant.

TABLE I

SOME NEUTRON ENERGIES FROM (d,n) REACTIONS

$E_i$ = 3.0 MeV $\theta = 30^\circ$

| TARGET | $^{12}C$ | $^{14}N$ | $^{16}O$ |
|---|---|---|---|
| Natural Abundance (%) | 98.89 | 99.63 | 99.759 |
| $Q(d,n_o)$ MeV (12) | - 0.281 | 5.066 | - 1.627 |
| Neutron Energy $n_o$ | 2.582 | 7.932 | 1.223 |
| $n_1$ | | 2.771 | 0.685 |
| $n_2$ | | 2.710 | |
| $n_3$ | | 1.763 | |
| $n_4$ | | 1.098 | |
| $n_5$ | | 1.033 | |
| $n_6$ | | 0.693 | |
| $n_7$ | | 0.235 | |

When carbon, nitrogen and oxygen are irradiated with a pulsed proton beam neutrons may be generated by (p,n) reactions, the Q-values of which are shown in Table II. It is obvious that (p,n) reactions on the isotopically abundant nuclides, carbon-12, nitrogen-14, oxygen-16 are much more endoergic than those on the heavier isotopes carbon-13, nitrogen-15, oxygen-17 and 18. Thus, it follows, that by suitably selecting the proton beam energy to induce (p,n) reactions, exclusively, on the heavier isotopes of carbon, nitrogen and oxygen, the determination of these isotopes by neutron time-of-flight spectrometry becomes possible, without interference from the more abundant, lighter nuclides.

This investigation was undertaken to study the conditions and limitations for the elemental determination of carbon, nitrogen and oxygen in the gaseous phase by neutron time-of-flight spectrometry, and the extent to which the method can be applied to the isotopic determination of the heavier isotopes of these elements.

TABLE II

NEUTRON ENERGIES FROM (p,n) REACTIONS

$E_p$ = 5.0 MeV  $\theta$ = 0°

| Target | $^{12}C$ | $^{13}C$ | $^{14}N$ | $^{15}N$ | $^{16}O$ | $^{17}O$ | $^{18}O$ |
|---|---|---|---|---|---|---|---|
| Natural Abundance (%) | 98.89 | 1.11 | 99.63 | 0.37 | 99.759 | 0.037 | 0.204 |
| Q(p,$n_0$) MeV (12) | -18.390 | -3.004 | -5.931 | -3.543 | -16.431 | -3.544 | -2.450 |
| Neutron Energy (MeV) | | | | | | | |
| $n_0$ | - | 1.941 | - | 1.381 | - | 1.390 | 2.495 |
| $n_1$ | | | | | | 0.854 | 1.555 |
| $n_2$ | | | | | | | 1.445 |
| $n_3$ | | | | | | | 1.406 |
| $n_4$ | | | | | | | 1.361 |
| $n_5$ | | | | | | | 0.744 |
| $n_6$ | | | | | | | 0.288 |

# C H A P T E R  II

## EXPERIMENTAL

## IRRADIATION BEAM

Pulsed proton and deuteron beams were obtained from the SUNI 5.5 MV Van de Graaff accelerator. The pulses were 5 nsec. long and 400 nsec. apart. In order to permit the results of different irradiations to be compared with one another, the beam current falling on a sample during an irradiation was integrated by means of a current integrator (13). In addition, the current was monitored with a standard $^{10}BF_3$-filled neutron counter placed about 1 metre from the target at $90^{o}$ to the direction of the incident bombarding beam. Average beam currents of less than 1 microamp were used to prevent damage to the thin nickel window (vide infra) which could not be cooled.

The following factors influenced the selection of the beam energy used for any particular irradiation:

(i) The energy of the neutrons generated by the bombarding beam had to be above the detection threshold of the measuring system.

(ii) The resolution of the time-of-flight system had to be adequate for the neutron energies of interest. Equation 6 shows that the resolution is best for low energy neutrons. Thus, low beam energies were used to promote better resolution because the energy of the neutrons decreased with decreasing energy of the bombarding particles.

(iii) The effect of the beam energy on the neutron yield

depends on the variation of reaction cross section with beam energy, the excitation function of the reaction. For analytical purposes the neutron yield per unit sample length should be as large as possible and should remain constant throughout the target. From a plot of the excitation function it can be deduced whether the neutron yield would change appreciably with changes in incident particle energy. Such neutron yield fluctuations are least when the slope of the excitation function is zero. However, provided the energy loss of the beam in the target were sufficiently small, the fluctuations in yield could be negligible so that the beam energy could be selected at a value for which the slope in the excitation curve is appreciably different from zero.

(iv) The higher the beam energy the greater the tendency for interfering reactions to occur, both in the target material and in all material in the vicinity of the beam. If the interfering reactions produce detectable neutrons, these will form a background against which the neutrons of interest have to be measured. Hence to reduce the background, the beam energy should be kept as low as possible.

## TARGETS

When solids or liquids are irradiated with charged particle beams, the entire energy of the beam is deposited

within a relatively short distance in the sample thus generating high temperatures, frequently sufficient to destroy the sample. This problem does not arise in the case of gases, because the density of a gas is so low that only a small fraction of the beam energy is transferred to the gas, per unit path length. For this reason charged particle irradiations could readily be carried out on gases, provided the container or gas cell had a sufficiently thin window through which the beam could enter.

Any energy spread suffered by the beam during its passage through the target and its container would cause uncertainty in the neutron energies and hence impair the resolution of the system. In addition, any change in the beam energy would result in a change in the reaction cross section and thus affect the neutron yield. Consequently, in order to reduce the energy loss of the beam only low pressure gaseous targets and relatively short containers were used in this investigation. A further advantage of the use of a short gas cell is the reduction in the uncertainty in the flight path and the consequent improved resolution (see equation 6).

## PREPARATION OF SAMPLES

### STANDARDS

All gases were handled in a glass vacuum apparatus shown diagrammatically in Figure 2. The apparatus consisted of a

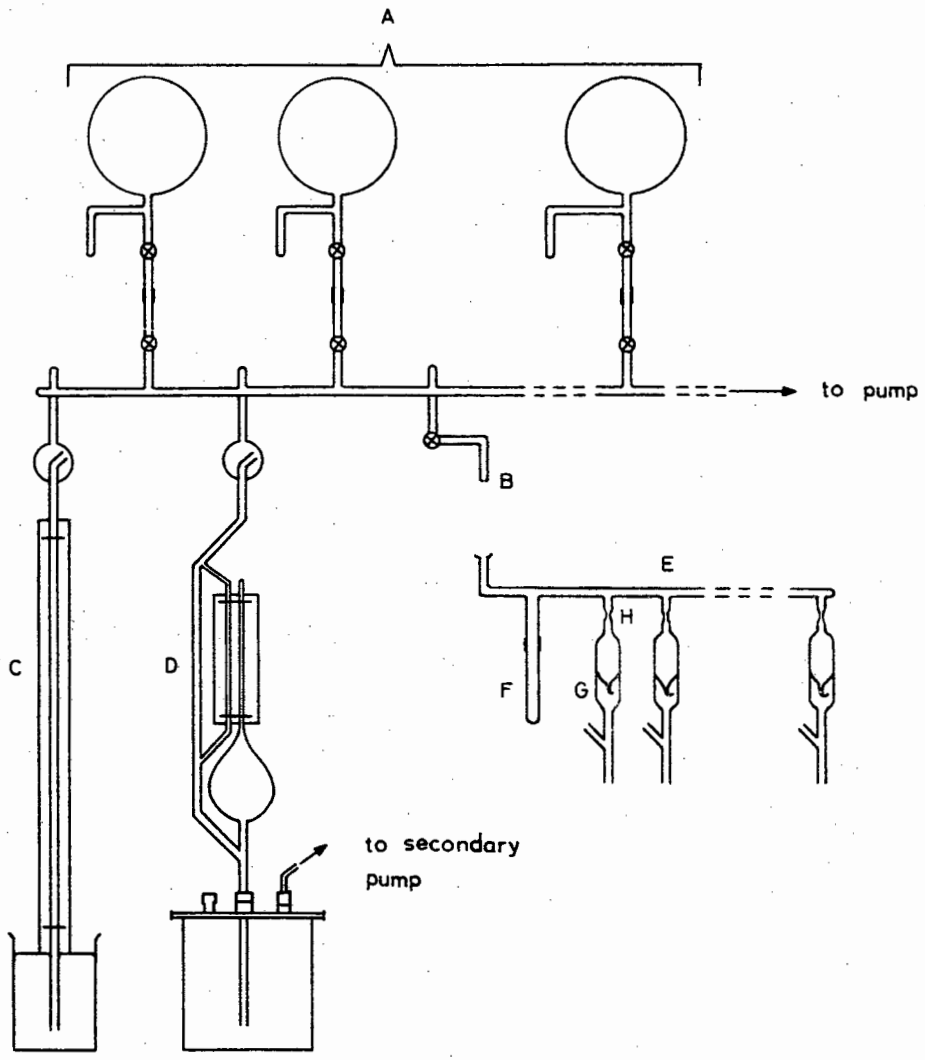


FIGURE 2. VACUUM APPARATUS

series of flasks, A, for storing and preparing gas samples. The gases were introduced at point B from gas cylinders. Relatively high pressures were measured on the calibrated manometer, C, and low pressures on the Mcleod Guage, D. The pumping system which is not shown in the diagram was capable of evacuating the apparatus to $4 \times 10^{-6}$mm. Hg and consisted of a silicone oil diffusion pump backed by a rotary oil pump. The diffusion pump was protected from condensable gases and mercury vapour by a liquid nitrogen trap.

Gases used as standards in this investigation were oxygen, nitrogen and methane. Pure oxygen and nitrogen were supplied by Messrs. African Oxygen and Acetylene Ltd., Cape Town. The Matheson Company, Inc., U.S.A., supplied 99.95% chemically pure methane as well as the pure and dry carbon dioxide and carbon monoxide used to prepare gaseous mixtures (vide infra).

Isotopically enriched oxygen-18, as chemically pure carbon dioxide containing 97.45 atom per cent $^{18}O$ and 0.27 atom per cent $^{17}O$, was supplied by Messrs Yeda Research and Development Company, Rehovoth, Israel. Enriched carbon-13, as chemically pure carbon dioxide containing 57.1 atom per cent $^{13}C$, and enriched nitrogen-15, as chemically pure ammonia containing 95 atom per cent $^{15}N$, were obtained from Messrs. Merck, Sharp and Dohme of Canada, Ltd., Montreal, Canada.

GASEOUS MIXTURES

When one of the components was not condensable it was possible to prepare mixtures of known composition by the following procedure: The vacuum apparatus shown in Figure 2 was evacuated and the condensable component was introduced into one of the flasks. A sample from this stock was distilled into another flask and its pressure measured on the mercury monometer. Thereafter, the flask was closed off and the residual gas in the vacuum line recondensed in the stock flask. With the measured sample frozen in the side arm of its flask, the non-condensable gas was introduced, its pressure recorded and the flask closed. As the pressure of both components was measured in the same volume, the composition of the gas mixture was given by the ratio of the partial pressures. In this way mixtures of carbon dioxide and nitrogen, and carbon dioxide and carbon monoxide were prepared.

The above procedure was not possible when isotopically enriched carbon dioxide and ammonia had to be diluted with the corresponding natural gas. In that case, after measuring the pressure of one component, the measured portion of the gas was quantitatively transferred to an empty flask, where it was stored until the second component had been similarly measured in the original volume. The two measured portions were mixed after any residual gas in the vacuum line had been removed.

LIQUID SAMPLES

Liquid samples were analysed by irradiating their vapours, which, previously, were freed from air. The removal of air from the vapours was carried out in the glass manifold, E, which was attached to the vacuum apparatus at the point B in Figure 2. To prevent condensation into the sample of components of the atmosphere in the manifold, the liquid sample, introduced into the system in the test tube, F, was first exposed to the vacuum pump before being frozen solid. Thereafter, the system was evacuated and the sample distilled into one of the units, G, which was then separated from the apparatus by sealing the glass with a flame at the point H. Inversion of the unit permitted placing a plunger in the side arm and attaching the unit to the irradiation assembly.

## IRRADIATION ASSEMBLY

A diagrammatic sketch showing the position of the irradiation cell and assembly relative to the beam is given in Figure 3. The whole irradiation assembly was insulated to permit measurement of the integrated beam current falling on a target during an irradiation. Care was taken to prevent sudden pressure changes on either side of the fragile nickel window of the cell. The dead space was made as small as possible to facilitate measurement of very small quantities of gas and to

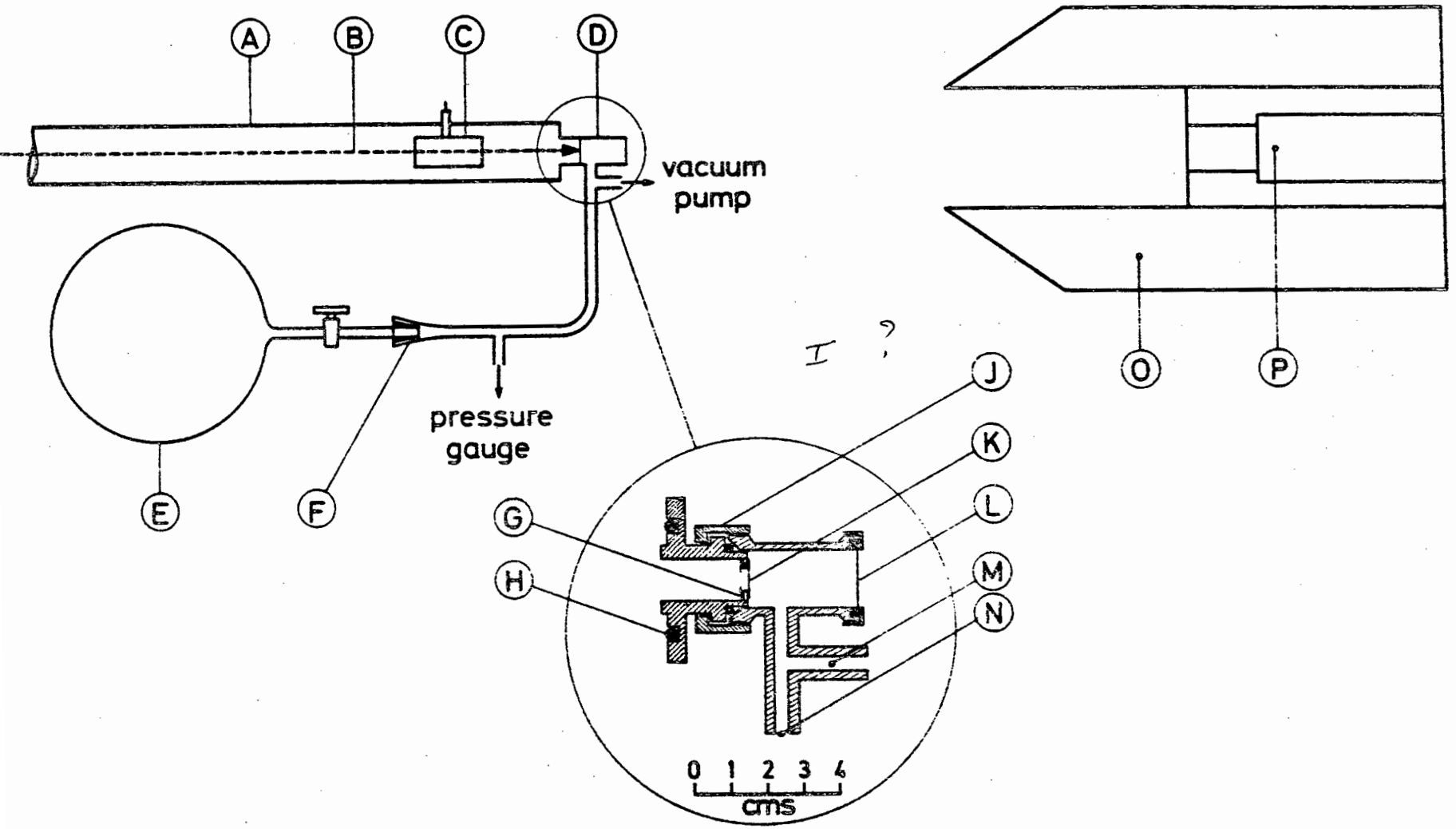


FIGURE 3. IRRADIATION ASSEMBLY

FIGURE 3.

Irradiation assembly and the irradiation cell

A. Beam tube

B. Irradiation beam

C. Pick-up probe

D. Irradiation cell

E. Gas sampling bottle

F. Sample connection point

G. Tantalum collimator and window support

H. Vacuum O-ring

I. Screw-on clamp

J. Nickel window

K. Platinum back of cell

L. Connection to vacuum pump

M. Connection to gas handling apparatus

N. Detector shield

O. Scintillation detector

minimise the loss of expensive sample gases not condensable with liquid nitrogen. The samples were introduced into the irradiation assembly at the glass-metal junction: gases could be inserted from a gas sampling bottle and liquids could be fed in by breaking the capillary seal with the magnetically operated plunger.

The pressure of the gas sample in the cell was measured with a transducer (Statham Instruments PA 731 model TC). The pressure media induced a signal from the transducer by causing a variation in the geometrical dimensions and consequently the resistance of one of the arms of a wheatstone bridge (see Figure 4). The induced signal was transmitted through an amplifier to a pen recorder. This system permitted the measurement of pressures in the range 0 to 100 mm Hg with a precision of $\pm$ 30 $\mu$, being largely determined by the quality of the amplifier.

## IRRADIATION CELL

The construction of the cell, used for samples which do not decompose under the irradiation conditions, is shown in Figure 3.

The nickel window, through which the irradiation beam passed, was mounted on a brass support with Araldite in such a way that the gas pressure in the cell acted on the window

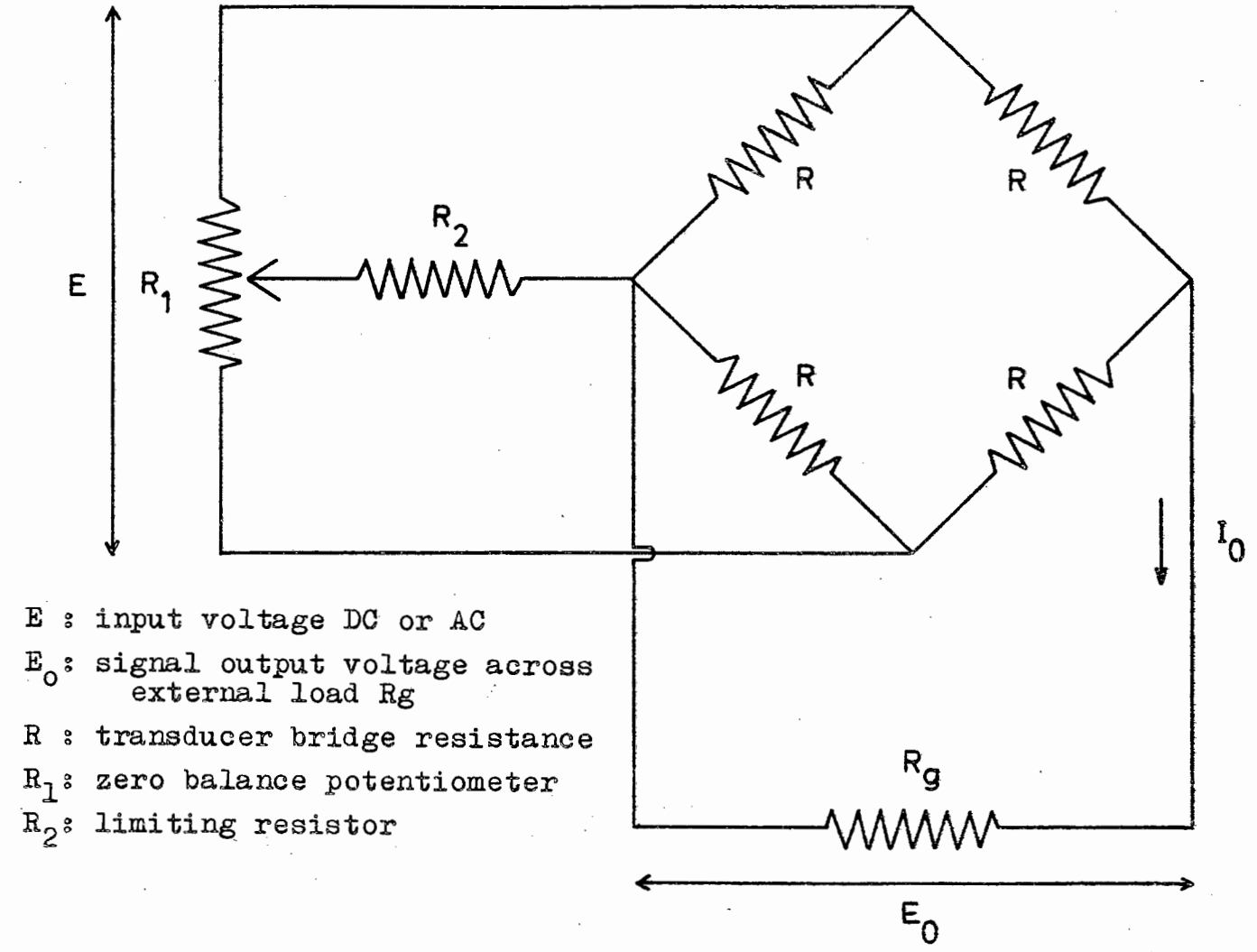


E : input voltage DC or AC

$E_o$: signal output voltage across external load Rg

R : transducer bridge resistance

$R_1$: zero balance potentiometer

$R_2$: limiting resistor

FIGURE 4. TYPICAL STRAIN GUAGE TRANSDUCER CIRCUIT

in the direction of the brass support. The window was about 2.5 μ thick and had a diameter of 6 mm. Any increase in the window thickness would cause an increase in the beam energy spread and consequently would have an adverse effect on the resolution of the measuring system. In addition, the energy of the irradiating beam would decrease and, consequently, the neutron yield from reactions of interest could be affected.

The rear wall of the cell and the beam collimators were made of tantalum, 0.25 mm. thick, which was sufficient to stop the beam completely. No interfering neutrons at low beam energies were formed by the tantalum. It had excellent thermal properties, was not fragile and was relatively inexpensive. To prevent the beam from striking the brass window support, the collimator nearest the irradiation cell had a diameter which was just less than that of the window. To promote dissipation of the heat generated by the beam, all the collimators were placed in contact with metal of the beam tube.

The body of the brass cell was made as short as possible in order to reduce the uncertainty in the flight path measurement ($\Delta d$ in equation 6). The best compromise between a short cell and the ease of manufacture was a cell about 3 cm. long. To simplify construction, the cell diameter was made slightly larger than the brass support of the nickel window.

## NEUTRON TIME-OF-FLIGHT SPECTROMETER

Neutrons generated by the pulsed beam in the target gas were detected in a cylindrical glass vessel (4 cm. thick and with a diameter of 12 cm.) filled with NE 213 scintillator supplied by Messrs. Nuclear Enterprises, Ltd., England. The detector was optically coupled to a 58 AVP Philips photo-multiplier tube, and was housed in a large shield mounted on a mobile tower, which could be attached to a pivot arm to facilitate its movement in a circular path about the target. The beam tube and the detector were about 3 metres above floor level.

### MEASURING ANGLE

The following factors influenced the selection of the measuring angle at which the neutron detector was placed during any particular irradiation:

(i) Nuclear reaction kinematics (equation 4) show how the mass of the target nuclide affects the variation of neutron energy with measuring angle. When neutrons are emitted from various target components of widely differing mass numbers, the resolution and identification of neutron energy groups may be facilitated by changing the angle at which the neutrons are measured. In the case of carbon, nitrogen and oxygen, this effect was relatively small because their mass numbers do not differ appreciably.

(ii) The effect of the measuring angle on the neutron yield may be deduced from angular distribution curves obtained for the relevant reactions at the bombarding energy in question. It is usually found that the angular distribution is a function whose value changes slowly with angle, but yields tend to be greatest for angles close to $0^{o}$.

(iii) It was observed that the number of background neutrons detected tends to drop more sharply with increasing angle of measurement than the neutron yield from the target. This effect can be used to increase the signal to noise ratio and is particularly useful when a deuteron beam is used. Most (d,n) reactions are endoergic so that neutrons may be generated wherever a deuteron beam strikes material along its path. Because the yield in the direction of the incident beam is greatest, and because the reaction sites occur along the length of the beam tube, the summed effect will be an extremely large neutron background in that direction relative to other directions of measurement. At a measuring angle of $30^{o}$ the background was largely reduced without sacrificing neutron yield from the reactions under investigation.

FLIGHT PATH LENGTH

The distance, d, of the neutron detector from the target largely determined the resolution of the detecting system which increased with increasing d. At the same time the number

of neutrons measured decreased with $d^2$. Hence for a particular irradiation the flight path was selected as the best compromise distance between the increase in resolution and the decrease in the neutron count rate. For most purposes a flight path of 3 metres was adequate.

ELECTRONIC EQUIPMENT (6)

A block diagram of the electronic equipment is shown in Figure 5. The fast signals from the neutron detector and the pick-up probe in the beam tube were fed into a time to amplitude converter (14) which generated a pulse directly proportional to the time interval between the two signals. A pulse height spectrum, linear in neutron flight time, was obtained and stored in a multichannel analyser. Low level electronic noise from the photomultiplier tube was eliminated by an energy discriminator. Because the neutron detector was sensitive to gamma-rays as well as neutrons, signals caused by gamma-rays were rejected by pulse shape discrimination (15). The effect of pulse shape discrimination on the time-of-flight spectrum of neutrons from (d,n) reactions on nitrogen-14 is shown in Figure 6. Coincidences between the slow outputs of the energy and shape discriminators were used to gate the multichannel analyser.

To ensure reproduceability of the relative efficiency of the detection system, particularly in the region near the

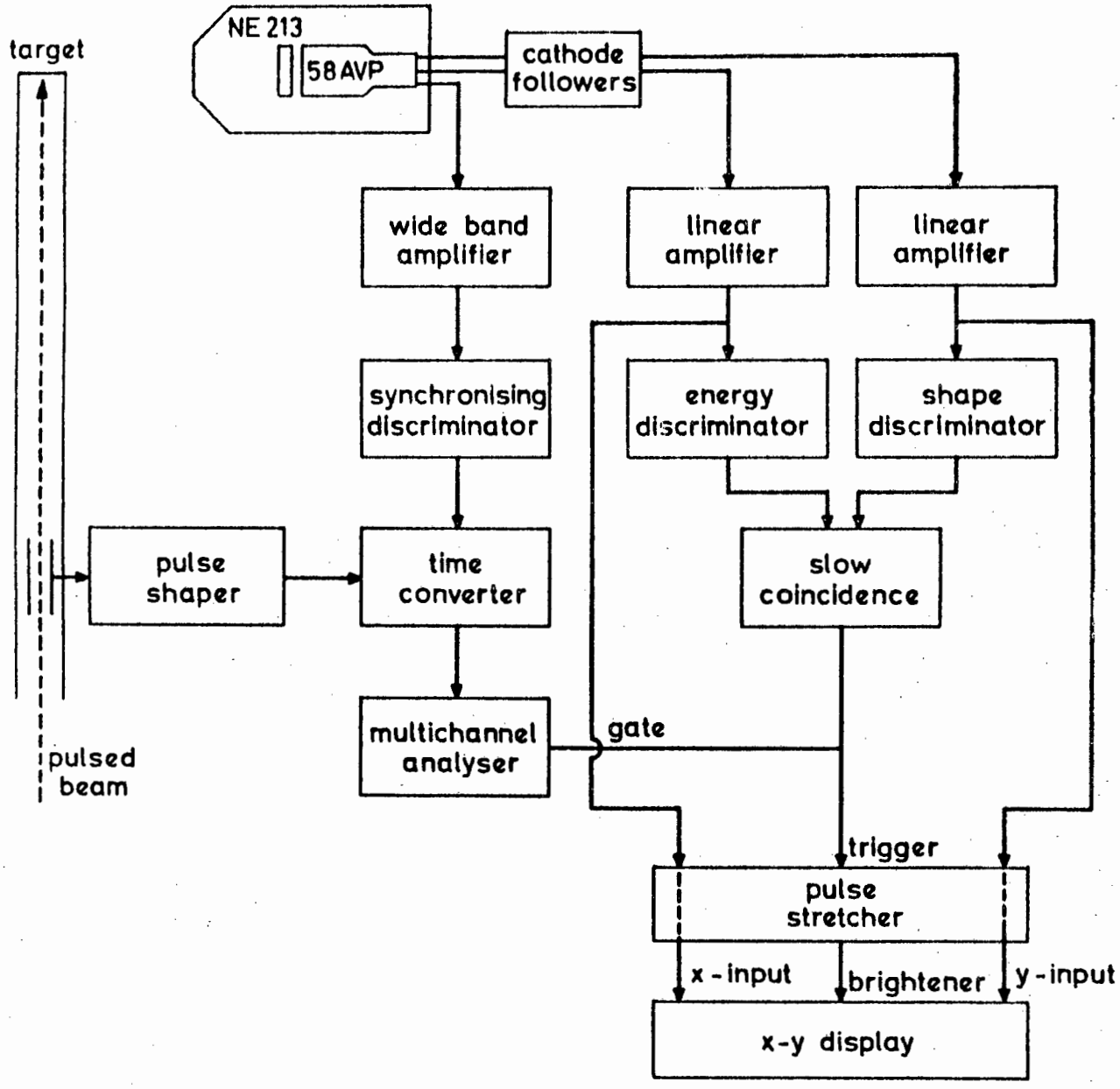


FIGURE 5. BLOCK DIAGRAM OF ELECTRONIC EQUIPMENT

(after McMurray, van der Merwe and van Heerden (15))

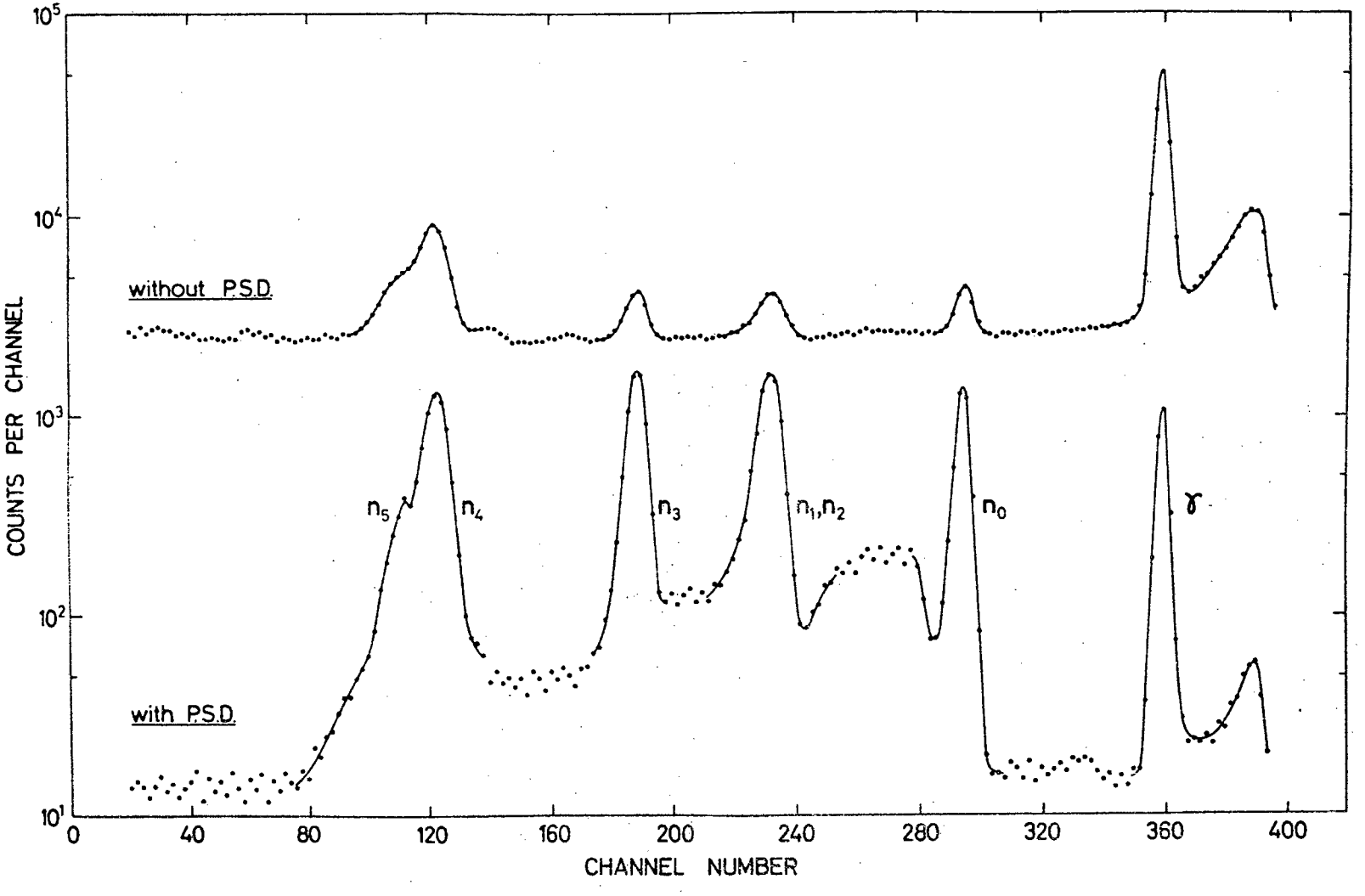


FIGURE 6. EFFECT OF PULSE SHAPE DISCRIMINATION ON THE TIME-OF-FLIGHT SPECTRUM OF NITROGEN

neutron detection threshold energy, a standard procedure was used to set up the equipment. The level of the linear energy bias was set on the photopeak of the 60 keV gamma ray from a standard americium-241 source placed in a reproduceable position in the detector housing. This setting corresponded to a neutron threshold of about 450 keV. A standard cobalt-60 gamma source and an americium-beryllium neutron source were used to set the pulse shape discrimination bias level, which was usually taken to be the level at which the cobalt-60 gamma-rays were just eliminated. Both bias levels were first coarsely set and then finely adjusted by measuring counting rates from the standard radioactive sources. The level of the discriminator on the fast pulses was set lower than that on the slow ones to ensure that the slow pulses determined the overall sensitivity of the system.

## DETECTOR EFFICIENCY

The variation of the relative efficiency of the neutron detector with neutron energy was obtained by comparing its response to that of a standard $^{10}BF_3$ long counter for neutrons of known energy from the $^{7}Li(p,n)^{7}Be$ reaction. The detector and long counter were placed at $+40^{o}$ and $-40^{o}$ to the direction of the beam respectively, and positioned so as to subtend the same solid angle at the target. By increasing the energy of the proton beam stepwise the variation of detector efficiency

with neutron energy could be obtained. The efficiency was measured twice: with the pulse shape discrimination operative and with it inoperative. The absolute efficiency of the $BF_3$ counter was obtained from tables (16). Figure 7 shows that the pulse shape discrimination affected the relative efficiency appreciably near the neutron energy threshold of the measuring system, that is at neutron energies of less than 1.5 MeV. Accordingly, every time the pulse shape discrimination was adjusted, the relative efficiency of the detector at low energies was checked prior to using the spectrometer.

## COUNTING CONDITIONS

The time interval covered between two successive channels in the multichannel analyser was adjusted by means of the time-to-amplitude converter. It was found that for the energy range of neutrons studied the time-of-flight spectrum generated in the analyser was adequate when the time difference between adjacent channels was about 1 nsec. The time scale of the spectra was calibrated, with the pulse shape discrimination inoperative, by inserting cables with accurately known delay times into the path of the electronic pulse to one of the inputs of the time-to-amplitude converter and noting the shift of the peak caused by the gamma-ray. The final, selected position of the peak representing the gamma-ray was used to determine the zero of the time scale.

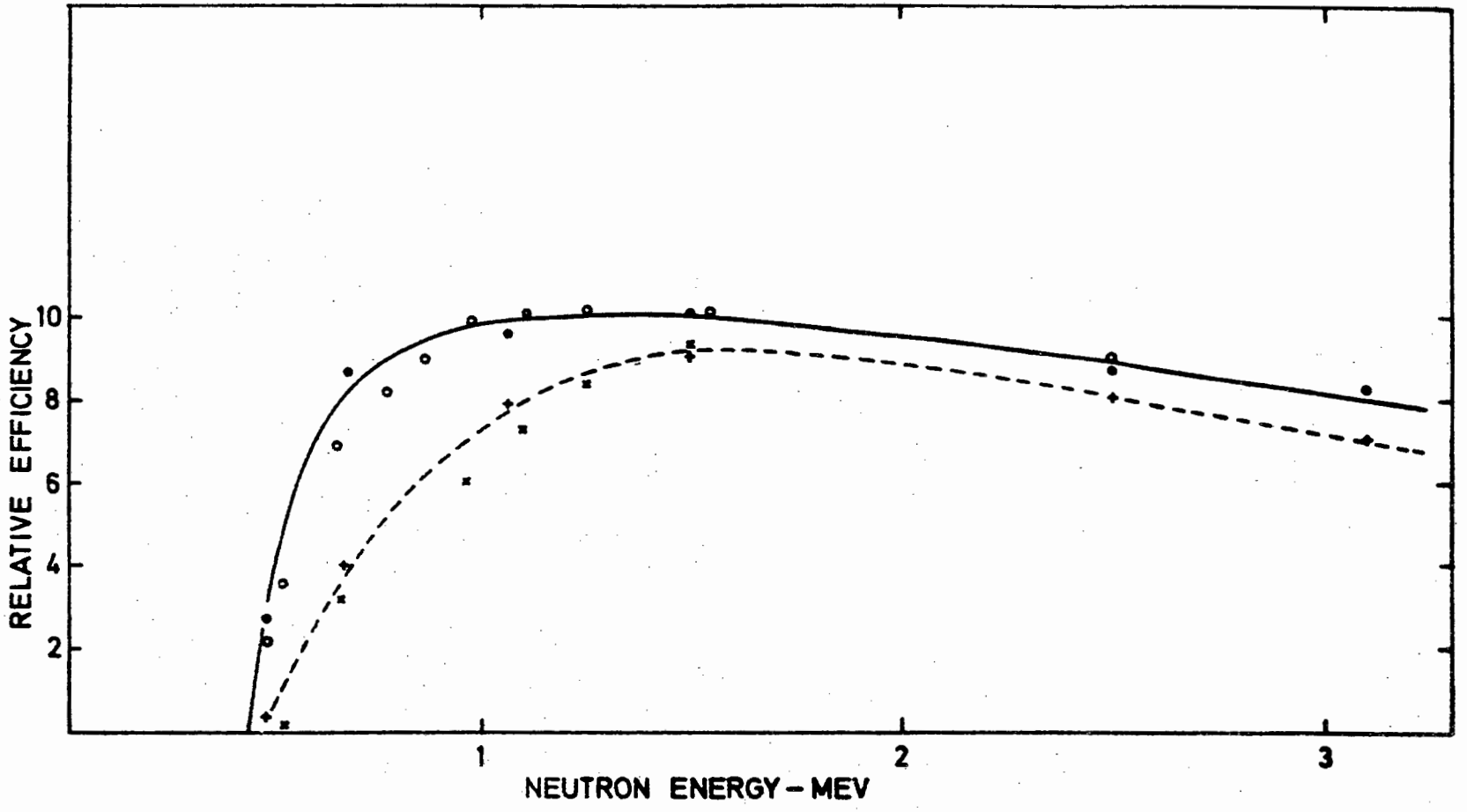


FIGURE 7. EFFECT OF PULSE SHAPE DISCRIMINATION ON THE RELATIVE DETECTOR EFFICIENCY

Solid line : with P.S.D. and dashed line : without P.S.D.

Even when the pulse shape discrimination is operative, not all the pulses generated by gamma-rays are eliminated. There is thus a residual peak in the neutron time-of-flight spectrum caused by gamma-rays generated at the target. The zero value on the time scale in all spectra was fixed relative to the position of this residual peak.

# C H A P T E R  III

# DETERMINATION OF CARBON, NITROGEN AND OXYGEN IN THERMALLY STABLE GASES

The successful elemental determination of carbon, nitrogen and oxygen by neutron time-of-flight spectrometry depends largely on whether characteristic neutron energy groups, suitable for analytical purposes, can be generated from isotopes of these elements. To provide a measure of the content of a nuclide in the target gas a characteristic neutron group should have an energy resolvable from that of neutrons produced by other components of the sample. Furthermore, to be detectable under the conditions of the experiment, such a neutron group should be produced by a nuclear reaction with sufficiently high cross section. Reference to Table I shows that, when carbon-12, nitrogen-14 and oxygen-16 are irradiated with a deuteron beam of 3 MeV, neutron groups will result with energies which permit the use of neutron time-of-flight spectrometry for their determination.

## NEUTRON SPECTRA

Typical neutron time-of-flight spectra obtained from methane, oxygen and nitrogen are given in Figure 8. The energy scale in that Figure is not linear because the spectra are based on time measurements with channel number proportional to the neutron flight time. For this reason, the peaks are spread over more channels towards the low energy ends of the spectra. The resolution (see equation 6) is limited by:

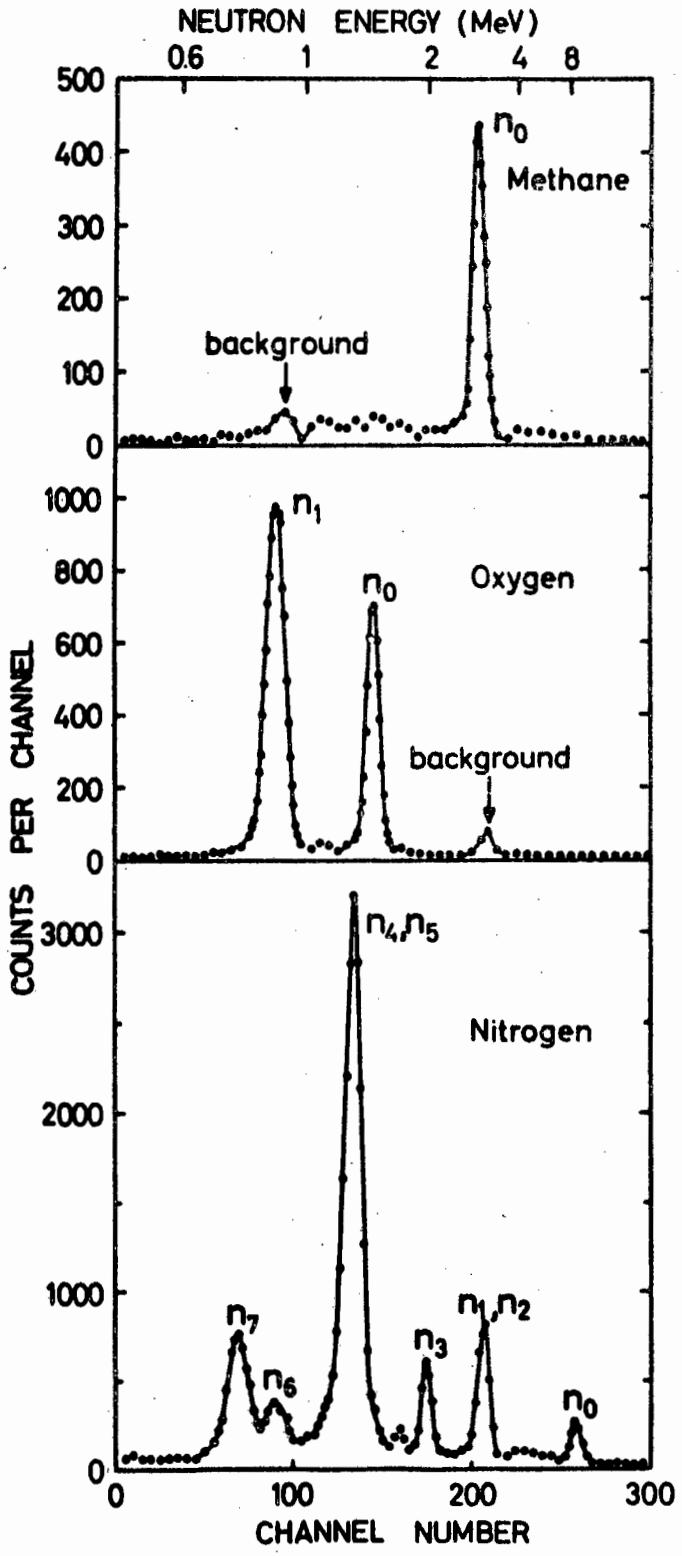


FIGURE 8. TYPICAL NEUTRON TIME-OF-FLIGHT SPECTRA

$E_d$ = 3.5 MeV
Flight path = 3.0 metres
$\theta$ = 30°

(i) the duration of the irradiation pulse which is largely responsible for the timing uncertainty in the measuring system,

(ii) the lengths of the gas cell and scintillation detector which together determine the uncertainty in the neutron flight path,

(iii) any energy lost by the irradiation beam in the gas sample.

The peaks in the spectra correspond to the energies listed in Table I, provided correction is made for the energy lost by the deuteron beam in the nickel window. Neutrons with energies below 700 keV could not be distinguished from gamma-rays by pulse shape discrimination. Accordingly, neutron groups which may have been expected from Table I, with energies below this value, were not observed.

From Figure 8 it is evident that carbon-12 produced only one characteristic neutron energy group which could be used to provide a measure of the carbon content of the sample. By contrast oxygen-16 gave rise to two neutron groups of which the $n_1$ group had an energy below 1 MeV. In this energy range the neutron detection efficiency decreased rapidly with decreasing neutron energy (see Figure 7). The number of neutrons counted would thus vary appreciably with fluctuations in neutron energy caused, for example, by the varying energy loss of the irradiation beam in samples of different pressure and composition.

In addition, because of low detection efficiency small changes in the neutron yield might not be reflected in the observed neutron count. For these reasons, the $n_1$ neutron group from oxygen-16 was not suitable for measurement and hence the $n_0$ group was used. Nitrogen-14 generated seven neutron groups. The spectrum shows that the neutron group pairs ($n_1$, $n_2$) and ($n_4$, $n_5$) were not resolvable under the conditions of measurement. This did not detract from their potential use as a measure of nitrogen content because the relative number of counts recorded from each neutron group remained constant provided the experimental parameters were not changed. However, the $n_1$ and $n_2$ groups had energies comparable with the energy of neutrons from carbon-12 and the $n_4$ and $n_5$ groups had energies similar to those of the $n_0$ neutrons from oxygen-16. The two groups $n_6$ and $n_7$ had energies near to the energy of the $n_1$ neutrons from oxygen-16 and occurred in the range of rapidly decreasing detector efficiency. These were, therefore, even less suitable for analytical purposes and consequently the $n_0$ and $n_3$ groups were used for determining the nitrogen content of a sample.

## CALIBRATION

The integrated count from a characteristic neutron energy group, as represented by the area under a peak in the spectrum,

is directly proportional to the pressure of the gas containing the nuclide under investigation, provided the experimental parameters remain undisturbed. The number of counts obtained from a selected neutron group was measured, and its variation with pressure served as a calibration curve for the determination of the nuclide. The calibration curves remained linear as long as the energy loss, depending on the pressure and composition of the gas sample, suffered by the beam during its passage through the target, was negligible. For an incident deuteron beam energy, $\underline{E}_d$, of 3.0 MeV and a measuring angle, $\theta$, of $30^{\circ}$ the number of counts obtained per millicoulomb of beam current per mm. pressure of methane, nitrogen and oxygen was 1743.3, 233.0 and 688.9 respectively. Under the conditions of the experiment the effective cross sections obtained from these figures for the reactions $^{12}C(d,n_0)^{13}N$, $^{14}N(d,n_0)^{15}O$, $^{16}O(d,n_0)^{17}F$ are in the ratios 14.99 : 1 : 2.96.

The calibration curves for nitrogen and carbon, shown in Figure 9, remained linear up to pressures of 100 mm. Hg, the maximum pressure used for analyses in this investigation. In particular, it is of interest to note that the curves are linear in the region 50 - 100 mm. Hg because in this pressure range the energy lost by the irradiation beam is already significant: for example, the energy lost by a 3 MeV deuteron beam in traversing a 3 cm. long cell containing carbon dioxide at 75 mm. pressure was calculated (17) to be 96 MeV. Energy

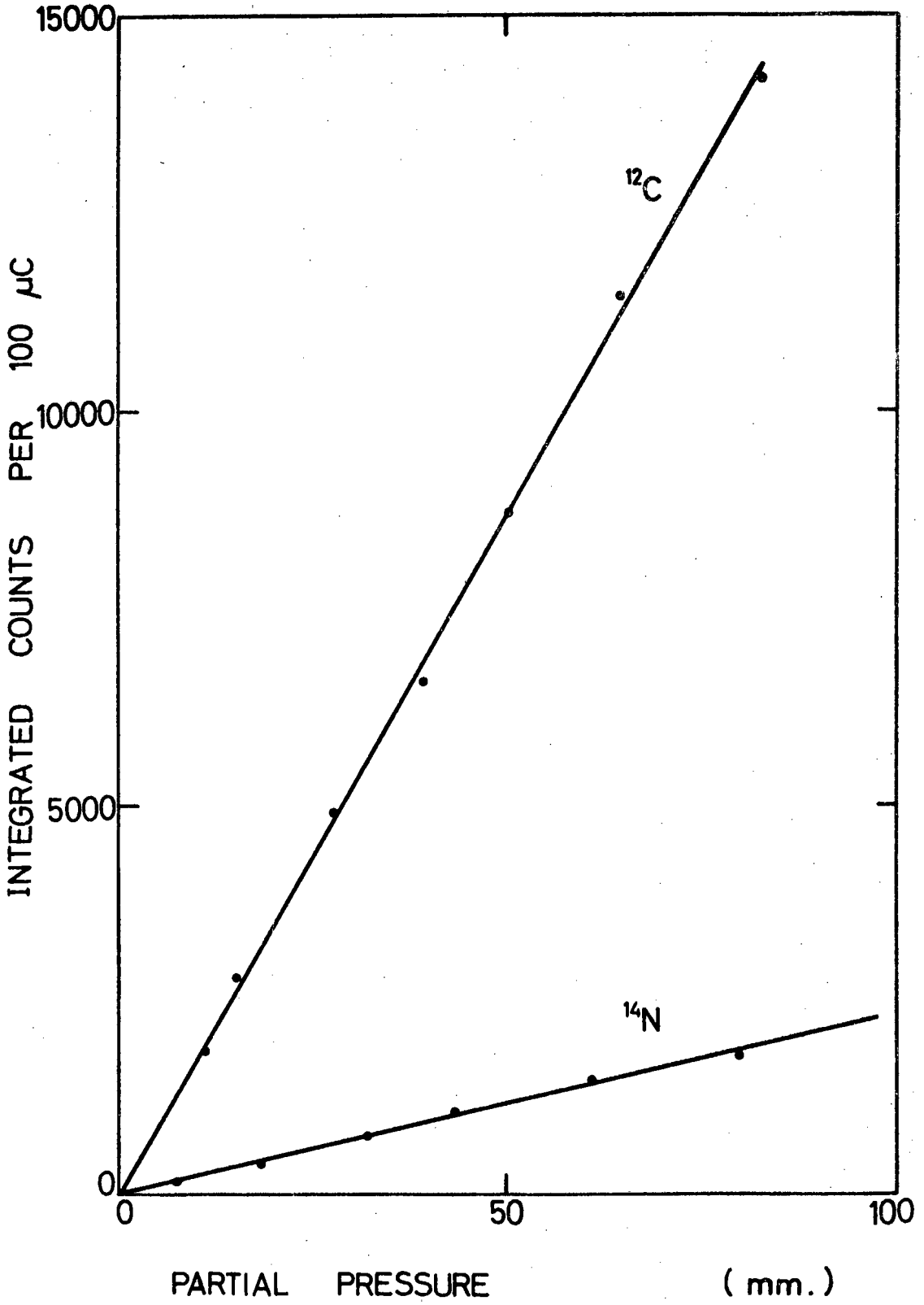


FIGURE 9. $^{12}C$ AND $^{14}N$ CALIBRATION CURVES

lost by the irradiation beam has three effects:

(i) The neutrons emitted will have lower energy and hence take a longer time to reach the detector. This effect manifests itself by a shift towards lower energies in the position of the peak in the spectrum.

(ii) The decrease in the neutron energy may affect the efficiency of neutron detection according to the efficiency curve shown in Figure 7.

(iii) At lower beam energies the relevant nuclear reaction may have a different cross section, thus affecting the neutron yield. The $^{12}C(n_0)$ and $^{14}N(n_0)$ neutron groups had observed energies of 2.375 MeV and 7.830 MeV respectively. At these energies, the energy range covered by one channel in the multichannel analyser is sufficiently wide to obscure any shift in the spectral peak. Furthermore, at these two energies, Figure 7 shows that the detector efficiency does not change appreciably for energy decreases of about 100 keV and hence these two effects would not be observable while measuring for calibration. Because the calibration curves for nitrogen-14 and carbon-12 remained linear at high gas target pressures it may be deduced that the cross sections for the reactions $^{12}C(d,n_0)^{13}N$ and $^{14}N(d,n_0)^{15}O$ do not vary appreciably, at 3 MeV, with the energy of the incident deuterons.

The oxygen-16 calibration curves obtained from measurements on carbon dioxide and oxygen are given in Figure 10.

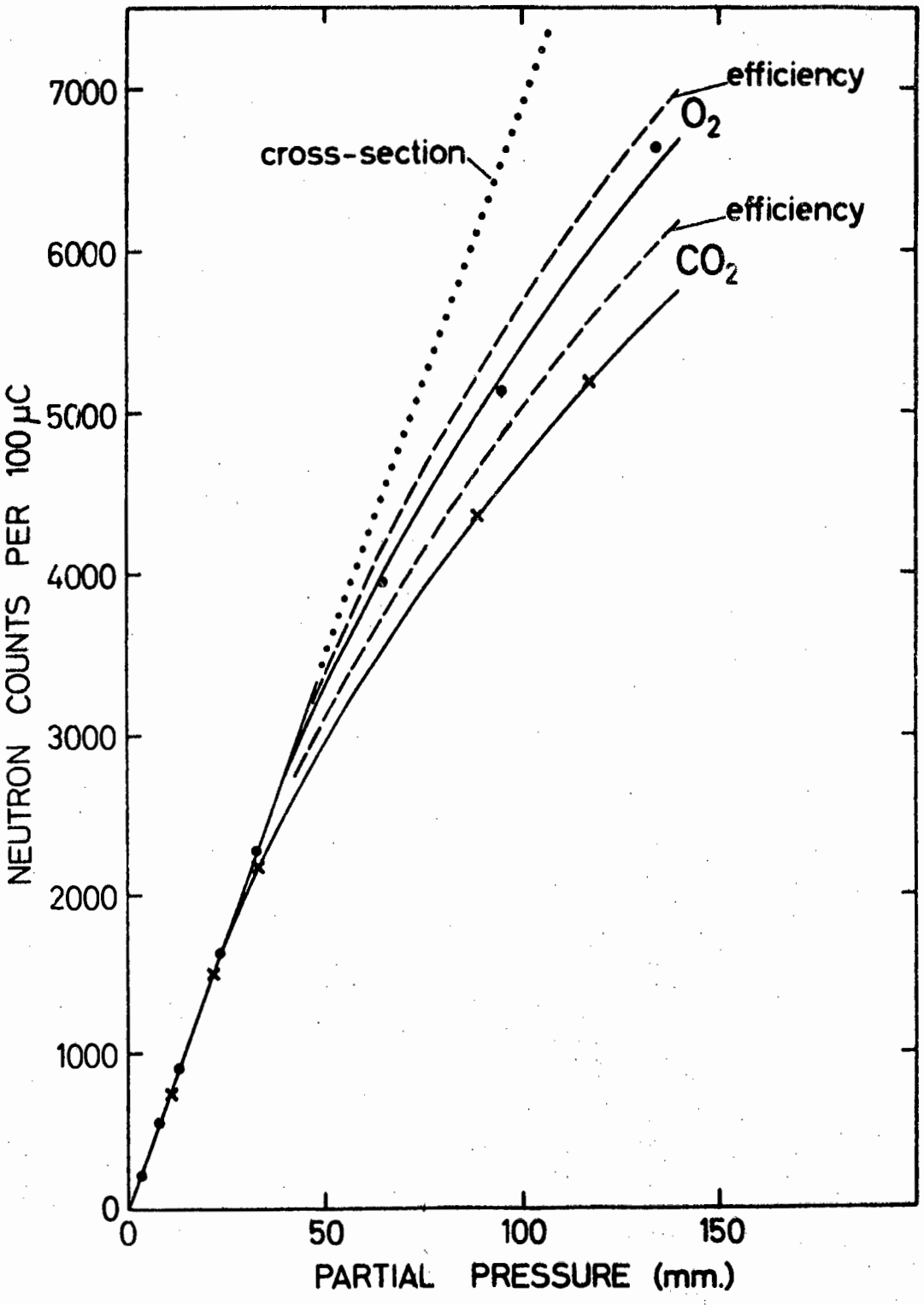


FIGURE 10. $^{16}O$ CALIBRATION CURVES FROM MEASUREMENTS ON $CO_2$ AND $O_2$

Experimental curves (solid), after correction from detector efficiency curve (dashed), and after correction from excitation function (dotted).

The two curves coincide and remain linear up to pressures of about 25 mm. Hg, but deviation from linearity occurs at higher pressures. The $^{16}O(n_0)$ neutrons had an observed energy of 1.039 MeV. At this neutron energy the energy range covered by one channel in the multichannel analyser was sufficiently small to observe a change in the position of the peak in the spectrum, but this shift did not affect the quantitative results because the integration limits were suitably adjusted. Figure 7 shows that at this neutron energy there is an appreciable change in detector efficiency with decreasing neutron energy, but when correction is made for the efficiency loss, the calibration curve still deviates from linearity as shown in Figure 10. It can thus be deduced that the effective cross section for the reaction $^{16}O(d,n_0)^{17}F$ decreases with decreasing deuteron beam energy at 3 MeV and this decrease is given in Figure 11. This conclusion is compatible with the fact that the calibration curve for oxygen-16 from measurements on carbon dioxide lies below that obtained from measurements on oxygen because the energy loss of the beam in the former is greater.

It follows from the above discussion that when carbon and nitrogen are to be determined in thermally stable gas mixtures, analysis may be performed at any pressure over the range studied. If oxygen is also to be determined the gas sample should be analysed at a pressure below 20 mm. Hg. After such

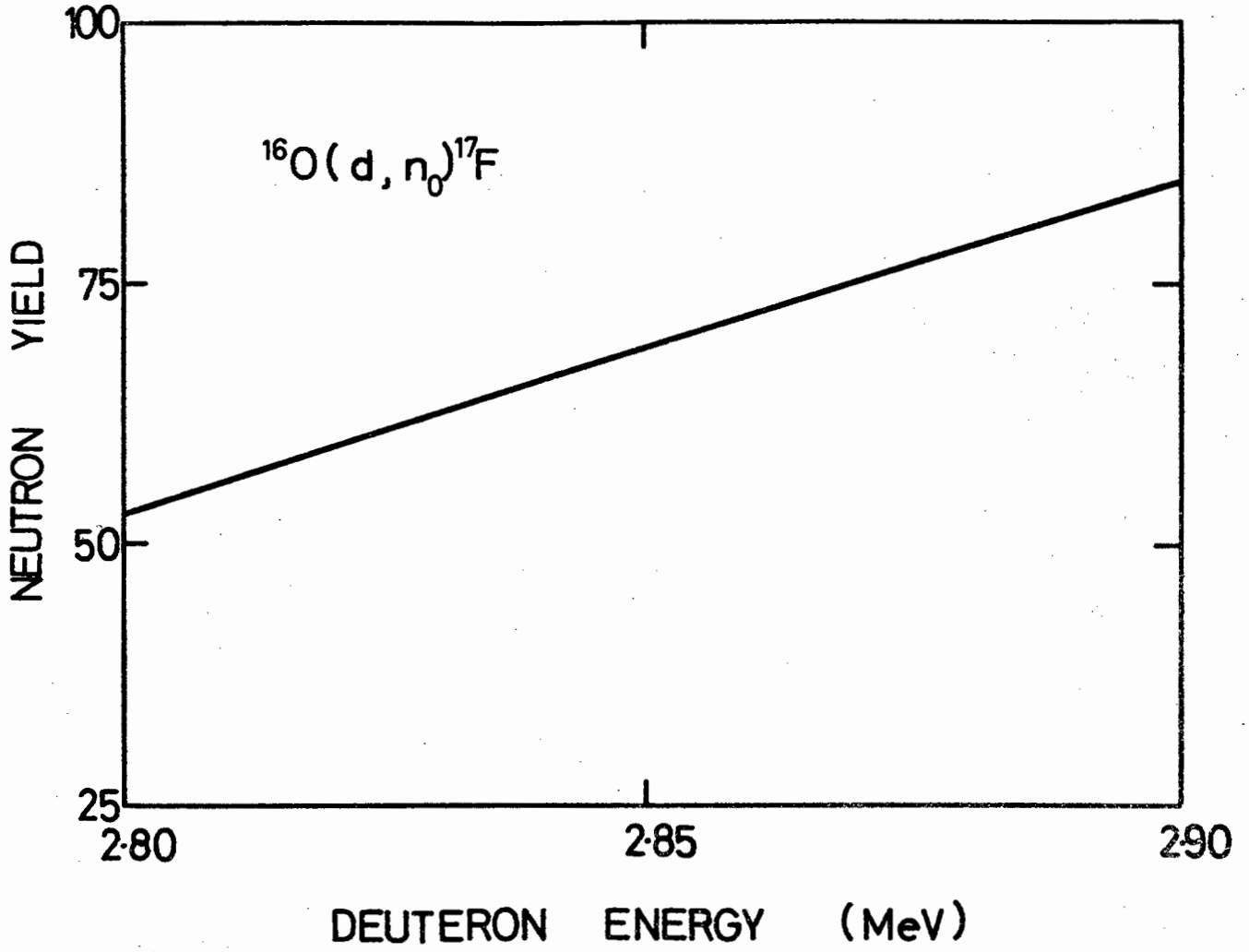


FIGURE 11. EXCITATION FUNCTION FOR THE $^{16}O(d,n_0)^{17}F$ REACTION

an analysis it may be found that an elemental component present in low concentration cannot be determined with sufficient precision. If the component is carbon or nitrogen the analysis may be repeated at a higher gas pressure, but if the low concentration component is oxygen, uncorrected neutron counts measured at higher pressures will lead to inaccurate results. However, the energy lost by the irradiation beam can be calculated from a knowledge of the concentrations of the major elemental components. Such a calculation will be adequately accurate because the oxygen content will not appreciably affect the energy lost by the beam. Hence correction for variations in detector efficiency and reaction cross section can be made from Figures 7 and 11 respectively.

## BACKGROUND

The predominant feature in the background spectra (a typical spectrum is given in Figure 12) was the peak corresponding to 2.5 MeV neutrons from carbon-12 due to the residual vacuum oil vapour in the beam tube which deposited on the hot spot generated at the point of incidence of the beam on the nickel window of the cell.

The background spectrum includes widened peaks of unknown origin. Such peaks may arise from neutrons produced by the interaction of the pulsed beam and material it strikes along

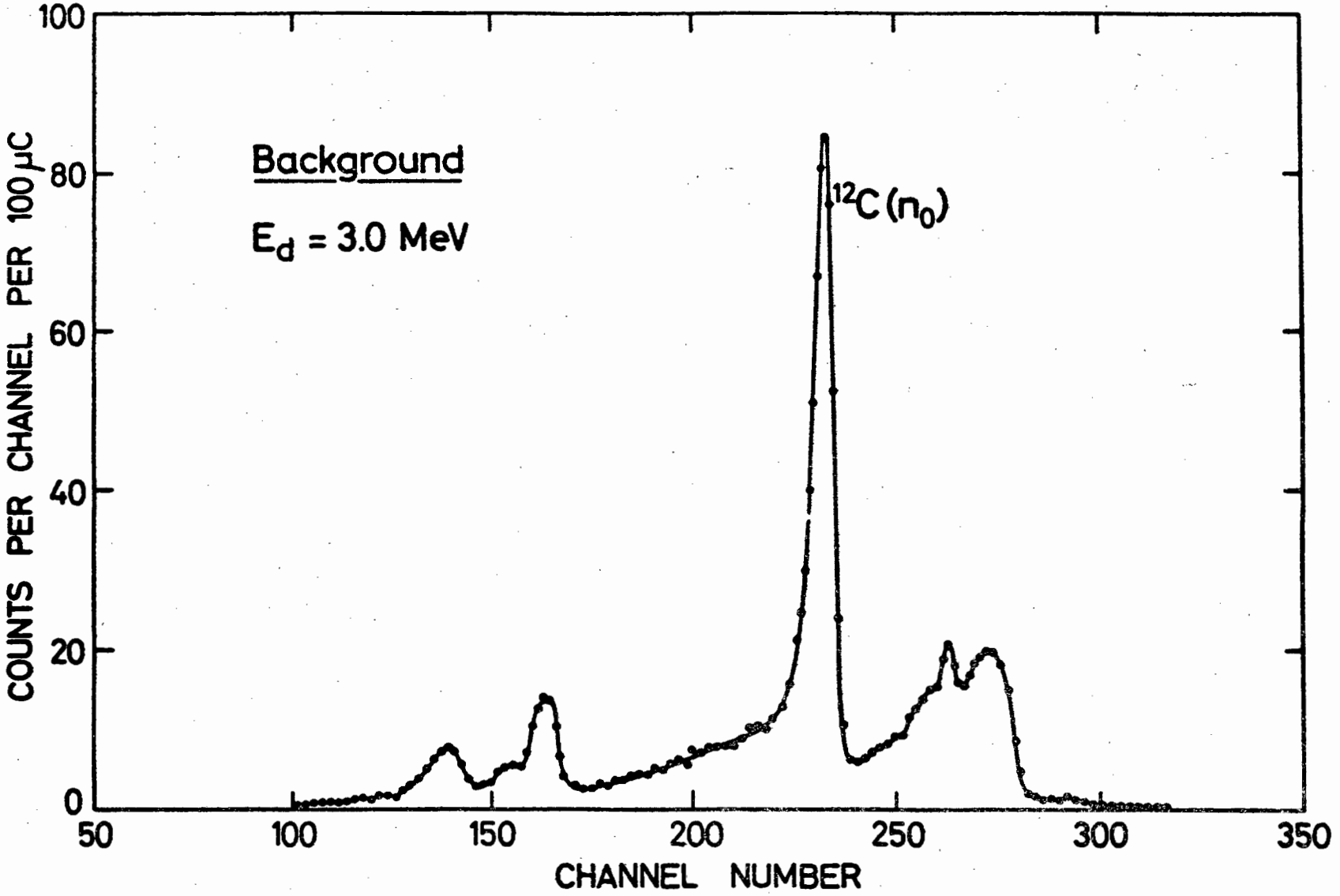


FIGURE 12. TYPICAL BACKGROUND SPECTRUM

$E_d$ = 3.0 MeV and $\theta = 30^\circ$ Flight path = 2.93 metres

the beam tube. Neutrons from these reaction sites would tend to arrive at the counter at regular time intervals and pulses from them would thus accumulate in the same channels of the multichannel analyser. Neutrons generated in the target but scattered into the detector would yield random pulses, the intensity of which would be a function of the total number of neutrons generated at the target. In extreme cases it may be necessary to correct for this background effect, which may be determined by irradiation of a sample with approximately the same composition and pressure as the one under analysis, but in which the component to be measured is absent.

## ANALYSIS OF GAS MIXTURES

A series of $CO_2/N_2$ mixtures were analysed to ascertain the ease with which each of the elements could be determined in the presence of the other two. A typical spectrum obtained from the irradiation of a $CO_2/N_2$ sample is given in Figure 13. It is evident that the $^{14}N(n_0)$ peak is well resolved from other peaks in the spectrum and therefore the number of counts under this peak was integrated and used as a measure of the nitrogen content of the mixture. The $^{14}N(n_1,n_2)$ neutron groups have energies comparable with the energy of the $^{12}C(n_0)$ group and the $^{14}N(n_4,n_5)$ neutron groups have energies comparable with those of $^{16}O(n_0)$ neutrons. Under constant experimental

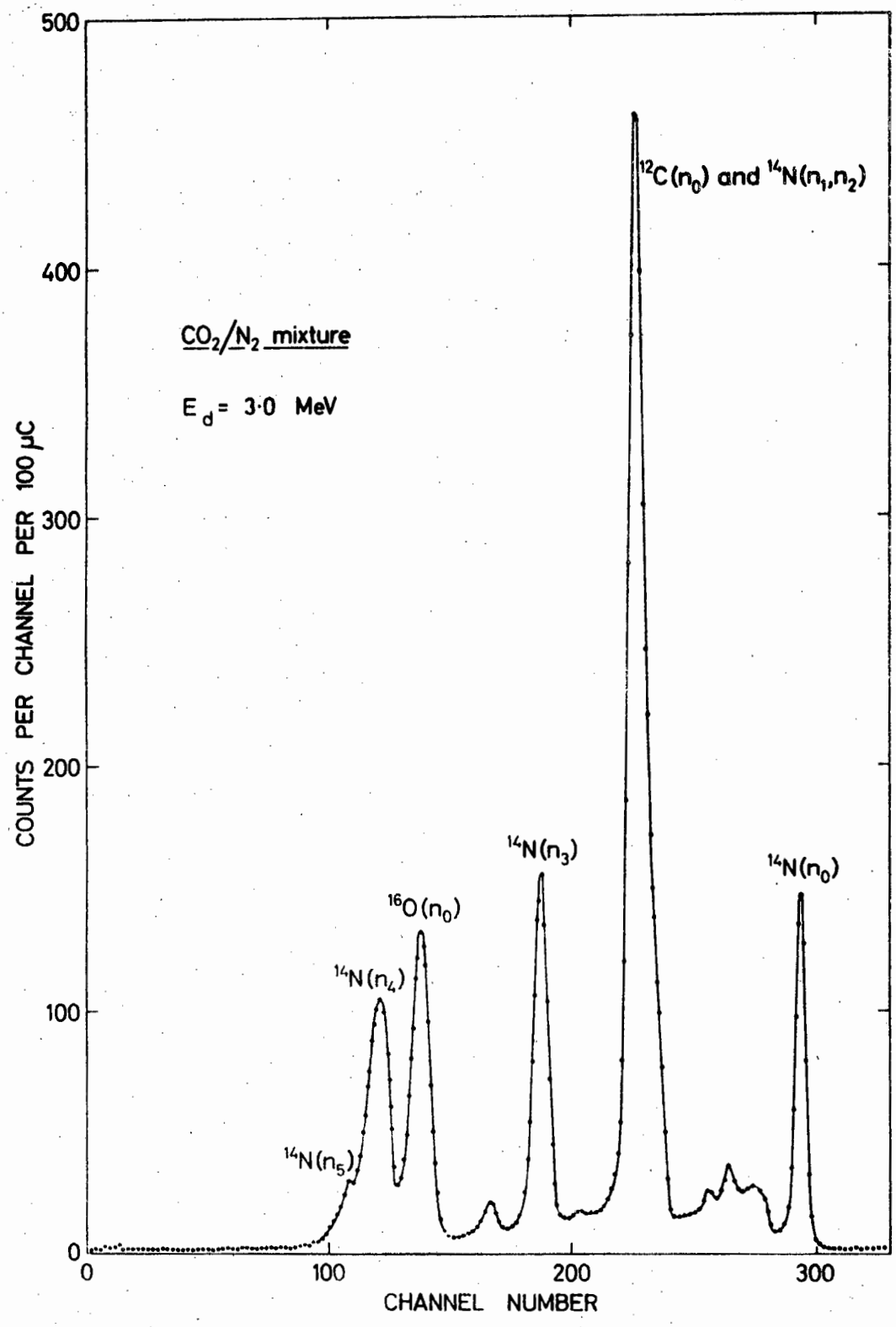


FIGURE 13. NEUTRON TIME-OF-FLIGHT SPECTRUM OF A $CO_2/N_2$ MIXTURE FOR $E_d$ = 3.0 MeV

$P_{CO_2}$ = 18.46 mm. $\theta$ = 30°

$P_{N_2}$ = 31.04 mm. Flight path = 2.93 metres

conditions, the number of counts obtained from the $^{14}N(n_1,n_2)$ and $(n_4,n_5)$ group pairs relative to the number of $^{14}N(n_0)$ neutrons is constant and could be determined from a spectrum of nitrogen gas. From a knowledge of these ratios and the number of $n_0$ neutrons from nitrogen-14, the nett neutron counts from $^{12}C(n_0)$ and $^{16}O(n_0)$ could be obtained. Because these analyses were carried out at 3 MeV, only one peak corresponding to neutrons from oxygen-16 is present (compare Figure 13 with Figure 8).

## RESULTS OF ANALYSES

The results of elemental analyses of gas mixtures containing carbon and oxygen are given in Table III and IV and the results of elemental analyses of gas mixtures containing carbon, nitrogen and oxygen are given in Tables V, VI, VII and VIII. Under each table the mean error, the relative standard deviation and the mean neutron count per 100 microcoulombs per unit pressure are given. These values are collected together in Table IX. The first value in Table V was omitted when calculating the standard deviation of 2.64% for the analysis of carbon-12 in the presence of nitrogen and oxygen. The apparent variation in the slope of the calibration curves of carbon-12 and oxygen-16 from one set of gas mixtures to the other reflects variations in the counting conditions used for the different analyses. In all cases the

TABLE III

SOME DETERMINATIONS OF CARBON IN $CO_2/CO$

$E_d$ = 3.0 MeV $\quad\quad$ $\theta$ = 30°

| Sample number | Total pressure in cell (20°C) | | Error | Relative error | Neutron counts per 100 μC | Neutron counts per 100 μC per mm. pressure |
|---|---|---|---|---|---|---|
| | Known A mm. | Found* B mm. | (B-A) | 100 X (B-A)/A | N | N/A |
| 78 | 89.70 | 92.40 | + 2.70 | + 3.01 | 16315 | 181.88 |
| 79 | 37.75 | 37.53 | - 0.22 | - 0.58 | 6453 | 170.95 |
| 85 | 40.75 | 41.63 | + 0.88 | + 2.16 | 7190 | 176.45 |
| 86 | 82.60 | 85.36 | + 2.76 | + 3.34 | 15046 | 182.15 |
| 87 | 40.17 | 39.33 | - 0.84 | - 2.09 | 6776 | 168.67 |
| 88 | 91.92 | 92.45 | + 0.53 | + 0.53 | 16324 | 177.58 |
| 89 | 41.55 | 41.19 | - 0.36 | - 0.87 | 7111 | 171.15 |
| 90 | 89.00 | 88.80 | - 0.19 | - 0.21 | 15669 | 176.06 |
| 91 | 37.67 | 37.19 | - 0.48 | - 1.27 | 6391 | 169.65 |
| 92 | 89.85 | 88.35 | - 1.50 | - 1.67 | 15588 | 173.49 |
| 93 | 35.12 | 36.14 | + 1.02 | + 2.90 | 6202 | 176.57 |
| 94 | 91.20 | 87.48 | - 3.72 | - 4.08 | 15432 | 169.21 |
| 95 | 38.70 | 38.17 | - 0.53 | - 1.37 | 6567 | 169.69 |

* Determined from $^{12}C(n_0)$ count

Mean error = + 0.0038 mm. Hg.

Mean neutron count per 100 μC per mm. total pressure = 174.12

Relative standard deviation = ± 2.27%

TABLE IV

SOME DETERMINATIONS OF OXYGEN IN $CO_2/CO$

$E_d$ = 3.0 MeV $\quad\quad$ $\theta$ = 30°

| Sample number | Partial pressure of oxygen (20°C) | | Error | Relative error | Neutron counts per 100 μC | Neutron counts per 100 μC per mm. pressure |
|---|---|---|---|---|---|---|
| | Known** A mm. | Found* B mm. | (B-A) | 100X (B-A)/A | N | N/A |
| 78 | 88.60 | 89.98 | + 1.38 | + 1.56 | 6707 | 75.70 |
| 79 | 37.29 | 37.78 | + 0.49 | + 1.31 | 2773 | 74.37 |
| 85 | 34.34 | 35.81 | + 1.47 | + 4.28 | 2625 | 76.43 |
| 86 | 62.97 | 64.37 | + 1.40 | + 2.22 | 4777 | 75.86 |
| 87 | 30.63 | 30.23 | - 0.40 | - 1.31 | 2204 | 71.96 |
| 88 | 61.45 | 59.75 | - 1.70 | - 2.77 | 4429 | 72.08 |
| 89 | 27.78 | 27.76 | - 0.02 | - 0.72 | 2018 | 72.66 |
| 90 | 56.41 | 56.58 | + 0.17 | + 0.30 | 4190 | 74.28 |
| 91 | 23.88 | 24.81 | + 0.93 | + 3.89 | 1796 | 75.22 |
| 92 | 49.61 | 47.29 | - 2.32 | - 4.68 | 3490 | 70.34 |
| 93 | 19.40 | 19.17 | - 0.23 | - 1.19 | 1371 | 70.69 |
| 94 | 46.52 | 44.61 | - 1.91 | - 4.11 | 3288 | 70.67 |
| 95 | 19.47 | 20.20 | + 0.73 | + 3.75 | 1448 | 74.37 |

** Calculated from $P_{O_2} \equiv 0.5P_{CO} + P_{CO_2}$

* Determined from $^{16}O(n_o)$ count

Mean error = - 0.0008 mm. Hg.

Mean neutron count per 100 μC per mm. pressure oxygen = 74.43

Relative Standard Deviation = ± 2.98%

TABLE V

SOME DETERMINATIONS OF CARBON IN $CO_2/N_2$

$E_d$ = 3.0 MeV $\theta = 30^\circ$

| Sample number | Partial pressure of oxygen (20°C) | | Error | Relative error | Neutron counts per 100 μC | Neutron counts per 100 μC per mm. pressure |
|---|---|---|---|---|---|---|
| | Known A mm. | Found* B mm. | (B-A) | 100X (B-A)/A | N | N/A |
| 99 | 4.54 | 5.70 | + 1.16 | + 25.55 | 807 | 177.75 |
| 100 | 8.74 | 9.13 | + 0.39 | + 4.46 | 1405 | 160.76 |
| 101 | 25.36 | 25.16 | - 0.20 | - 0.79 | 4199 | 165.58 |
| 104 | 48.28 | 46.94 | - 1.34 | - 2.78 | 7997 | 165.64 |
| 105 | 39.71 | 38.36 | - 1.35 | - 3.40 | 6501 | 163.71 |
| 106 | 55.30 | 55.41 | + 0.11 | + 0.20 | 9472 | 171.28 |
| 107 | 47.35 | 46.39 | - 0.96 | - 2.03 | 7901 | 166.86 |
| 108 | 67.02 | 67.83 | + 1.21 | + 1.21 | 11638 | 173.65 |
| 110 | 72.97 | 74.32 | + 1.35 | + 1.85 | 12770 | 175.00 |

* Determined from $^{12}C(n_0)$ count

Mean Error = - 0.0033 mm. Hg.

Mean neutron count per 100 μC per mm. pressure $CO_2$ = 168.91

Relative standard deviation = 2.64%

TABLE VI

SOME DETERMINATIONS OF NITROGEN IN $CO_2/N_2$

$E_d$ = 3.0 MeV $\quad\quad$ $\theta$ = 30°

| Sample number | Partial pressure of nitrogen (20°C) | | Error | Relative error | Neutron counts per 100 μC | Neutron counts per 100 μC per mm. pressure |
|---|---|---|---|---|---|---|
| | Known A mm. | Found* B mm. | (B-A) | 100 X (B-A)/A | N | N/A |
| 97 | 93.11 | 89.69 | - 3.42 | - 3.67 | 2130 | 22.88 |
| 98 | 69.22 | 69.43 | + 0.21 | + 0.30 | 1658 | 23.95 |
| 99 | 88.46 | 89.60 | + 1.14 | + 1.29 | 2128 | 24.06 |
| 100 | 80.06 | 80.29 | + 0.23 | + 0.29 | 1911 | 23.87 |
| 101 | 58.63 | 60.29 | + 1.66 | + 2.83 | 1455 | 24.65 |
| 102 | 35.74 | 33.63 | - 2.11 | - 5.90 | 824 | 23.06 |
| 103 | 31.04 | 28.61 | - 2.43 | - 7.83 | 707 | 22.78 |
| 104 | 49.72 | 52.69 | + 2.97 | + 5.97 | 1268 | 25.50 |
| 105 | 40.89 | 41.44 | + 0.55 | + 1.35 | 1006 | 24.60 |
| 106 | 37.90 | 39.51 | + 1.61 | + 4.25 | 961 | 25.36 |
| 107 | 32.45 | 34.36 | + 1.91 | + 5.89 | 841 | 25.92 |
| 108 | 27.57 | 26.12 | - 1.45 | - 5.26 | 649 | 23.54 |
| 110 | 17.93 | 17.11 | - 0.82 | - 4.57 | 439 | 24.48 |

* Determined from $^{14}N(n_0)$ count

Mean error = + 0.0039 mm. Hg.

Mean neutron count per 100 μC per mm. pressure $N_2$ = 24.20

Relative standard deviation = ± 4.64%

TABLE VII

SOME DETERMINATIONS OF OXYGEN IN $CO_2/N_2$

$E_d$ = 3.0 MeV $\theta$ = 30°

| Sample number | Partial pressure of oxygen (20°C) | | Error | Relative error 100X | Neutron counts per 100 μC | Neutron counts per 100 μC per mm. pressure |
|---|---|---|---|---|---|---|
| | Known A mm. | Found* B mm. | (B-A) | (B-A)/A | N | N/A |
| 99 | 4.54 | 4.72 | + 0.18 | + 3.96 | 327 | 72.03 |
| 100 | 8.74 | 8.23 | - 0.51 | - 5.84 | 569 | 65.10 |
| 101 | 25.36 | 25.81 | + 0.45 | + 1.77 | 1780 | 70.19 |
| 102 | 21.26 | 21.64 | + 0.38 | + 1.79 | 1493 | 70.23 |
| 103 | 18.46 | 17.87 | - 0.59 | - 3.20 | 1233 | 66.79 |
| 104 | 48.28 | 50.07 | + 1.79 | + 3.71 | 3451 | 71.48 |
| 105 | 39.71 | 40.51 | + 0.80 | + 2.01 | 2793 | 70.33 |
| 106 | 55.30 | 53.90 | - 1.40 | - 2.53 | 3715 | 67.18 |
| 107 | 47.35 | 45.49 | - 1.86 | - 3.93 | 3136 | 66.23 |
| 108 | 67.02 | 69.05 | + 2.03 | + 3.03 | 4759 | 71.01 |
| 110 | 72.97 | 71.68 | - 1.29 | - 1.77 | 4940 | 67.70 |

* Determined from $^{16}O(n_0)$ count

Mean error = - 0.0018 mm. Hg.

Mean neutron count per 100 μC per mm. pressure $CO_2$ = 69.78

Relative standard deviation = ± 3.44%

TABLE VIII

SOME DETERMINATIONS OF NITROGEN IN $CO_2/N_2$

$E_d$ = 2.0 MeV $\theta$ = 30°

| Sample number | $N_2$ Partial Pressure(20°) | | Error | Relative error | Neutron counts per 100μC | Neutron counts per 100μC per mm. pressure |
|---|---|---|---|---|---|---|
| | Known A mm. | Found* B mm. | (B-A) | 100 X (B-A)/A | N | N/A |
| 141 | 11.85 | 12.08 | + 0.23 | + 1.94 | 266.0 | 22.45 |
| 138 | 19.61 | 20.21 | + 0.60 | + 3.06 | 458.4 | 23.38 |
| 140 | 20.22 | 20.88 | + 0.58 | + 2.87 | 472.4 | 23.36 |
| 135 | 21.88 | 21.79 | - 0.09 | - 0.41 | 495.8 | 22.66 |
| 139 | 23.42 | 23.55 | + 0.13 | + 0.56 | 537.4 | 22.95 |
| 136 | 33.72 | 33.18 | - 0.54 | - 1.60 | 765.4 | 22.70 |
| 67 | 44.70 | 45.11 | + 0.41 | + 0.92 | 1047.6 | 23.44 |
| 68 | 51.95 | 50.22 | - 1.73 | - 3.33 | 1168.6 | 22.50 |
| 69 | 60.35 | 56.66 | - 3.69 | - 6.11 | 1321.0 | 21.90 |
| 70 | 73.95 | 77.59 | + 3.64 | + 4.92 | 1816.0 | 24.56 |

* Determined from $^{14}N(n_0)$ count

Mean error = - 0.05 mm. Hg.

Mean neutron count per 100 microcoulombs per mm. pressure = 22.99

Relative standard deviation = ± 3.29%

TABLE IX

SUMMARY OF RESULTS OF ELEMENTAL ANALYSES

| Gas Mixture | Nuclide | $E_d$ MeV | Number of samples | Slope of calibration line* | Mean neutron count per 100μC per mm. pressure | Mean error mm. Hg. | Relative Standard Deviation % |
|---|---|---|---|---|---|---|---|
| $CO_2/CO$ | $^{12}C$ | 3.0 | 13 | 179.76 | 174.12 | + 0.0038 | ± 2.27 |
| | $^{16}O$ | 3.0 | 13 | 75.36 | 74.43 | - 0.0008 | ± 2.98 |
| $CO_2/N_2$ | $^{12}C$ | 3.0 | 9 | 174.33 | 168.91 | - 0.0033 | ± 2.64 |
| | $^{14}N$ | 3.0 | 13 | 23.30 | 24.20 | + 0.0039 | ± 4.64 |
| | $^{16}O$ | 3.0 | 11 | 68.89 | 69.78 | - 0.0018 | ± 3.44 |
| | $^{14}N$ | 2.0 | 10 | 23.66 | 22.99 | - 0.0460 | ± 3.29 |

* Counts per 100μC per mm. pressure.

mean neutron count is in excellent agreement with the slope of the calibration curve within the precision of the method. The very low mean errors indicate that the method is accurate and a statistical evaluation of each group of determinations shows that the method is free from bias.

The relative standard deviation of the method is about ± 3% for all three elements. Comparison of the standard deviations for the two carbon-12 cases and the two oxygen-16 cases show that in the absence of nitrogen the standard deviation of the method is lower.

When nitrogen is present, the additional corrections required to obtain the nett counts make a significant contribution to the total variance of the determinations resulting in higher relative standard deviations. The determination of nitrogen with a 2 MeV, rather than a 3 MeV, deuteron beam precluded the detection of neutrons from oxygen-16 (see Figure 14) and resulted in a comparatively lower value of the $^{12}C(n_0)$ count and of the background continuum in the energy range corresponding to $n_0$ neutrons from nitrogen-14. It is of interest to note that at the lower incident deuteron energy the $^{14}N(n_1)$ and $(n_2)$ neutron energy groups are partially resolvable. A series of nitrogen determinations in samples containing carbon and oxygen with a 2 MeV deuteron beam had a relative standard deviation of ±3.29%. When the same determinations were carried out with a 3 MeV deuteron beam the higher

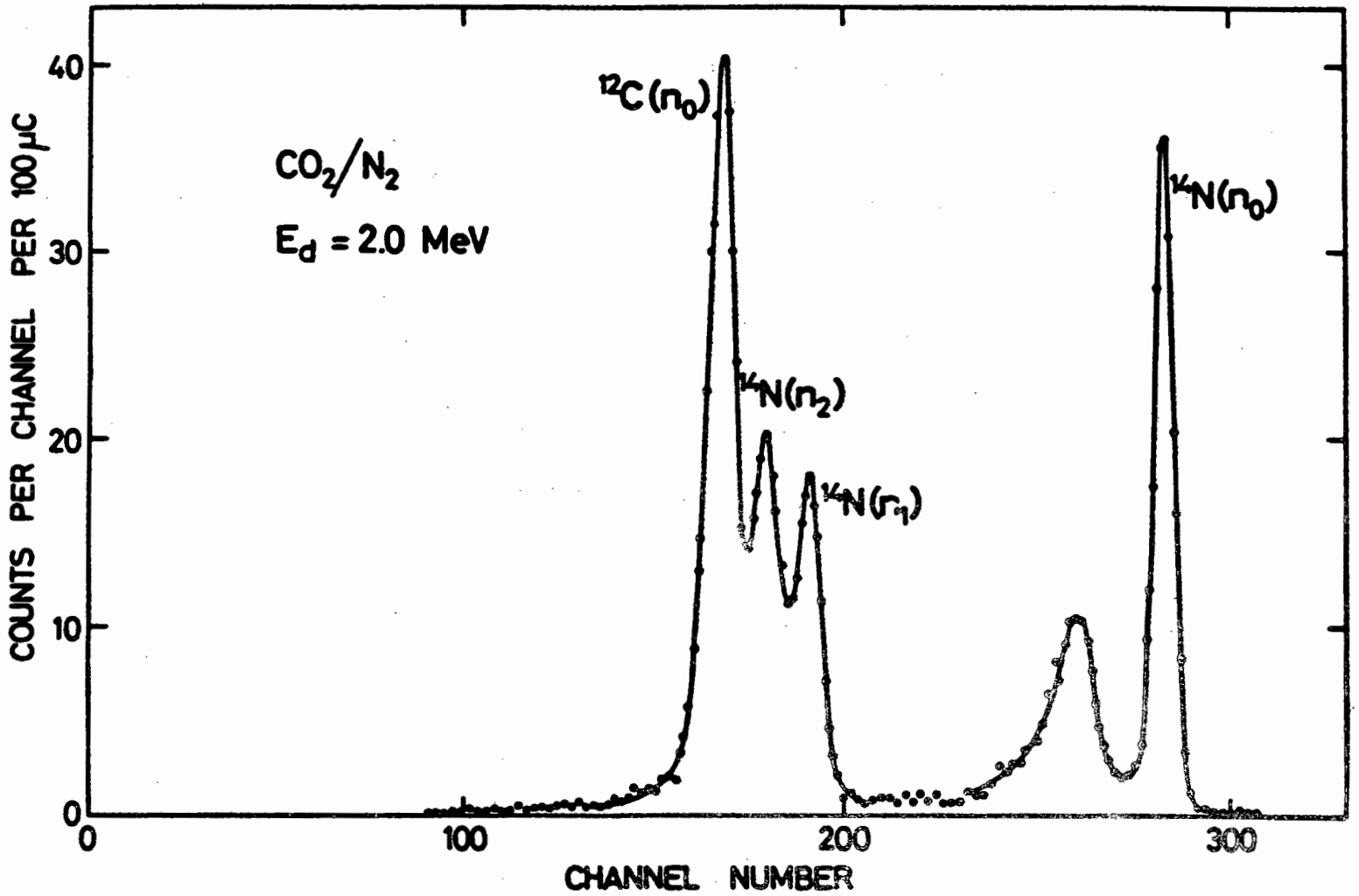


FIGURE 14. NEUTRON TIME-OF-FLIGHT SPECTRUM OF A $CO_2/N_2$ MIXTURE FOR $E_d$ = 2.0 MeV

$P_{CO_2}$ = 11.66 mm. $\theta = 30^\circ$

$P_{N_2}$ = 19.61 mm. Flight path = 2.93 metres

background continuum caused a statistical error which was reflected in the higher relative standard deviation of 4.64%. Comparison of the standard deviations for the analyses of the three elements shows that better results, i.e. lower relative standard deviations, were obtained when the nuclear reaction used in the determination had a higher cross section. This was specially evident in the case of carbon, despite the fact that the background corresponding to the energy of the carbon neutrons was greatest.

When mixtures of two known gases containing the same elements in different stoichiometric proportions are to be analysed, the concentration of each gas in the mixture can be deduced from a knowledge of the atom ratio of the component elements. Such a determination was carried out for carbon and oxygen in mixtures of carbon monoxide and carbon dioxide and the results are given in Figure 15. As the determination of each element is subject to its own errors, the error in the ratio would be given by:

$$\frac{\sigma_Q}{Q} = \sqrt{\left(\frac{\sigma_1}{R_1}\right)^2 + \left(\frac{\sigma_2}{R_2}\right)^2} \quad \ldots\ldots\ldots\ldots \quad (7)$$

where $\underline{Q}$ is the quotient of $\underline{R}_1$ and $\underline{R}_2$ and $\sigma_Q$, $\sigma_1$ and $\sigma_2$ are the standard deviations corresponding to $\underline{Q}$, $\underline{R}_1$ and $\underline{R}_2$ respectively. The sizes of the errors indicated in Figure 15 were calculated

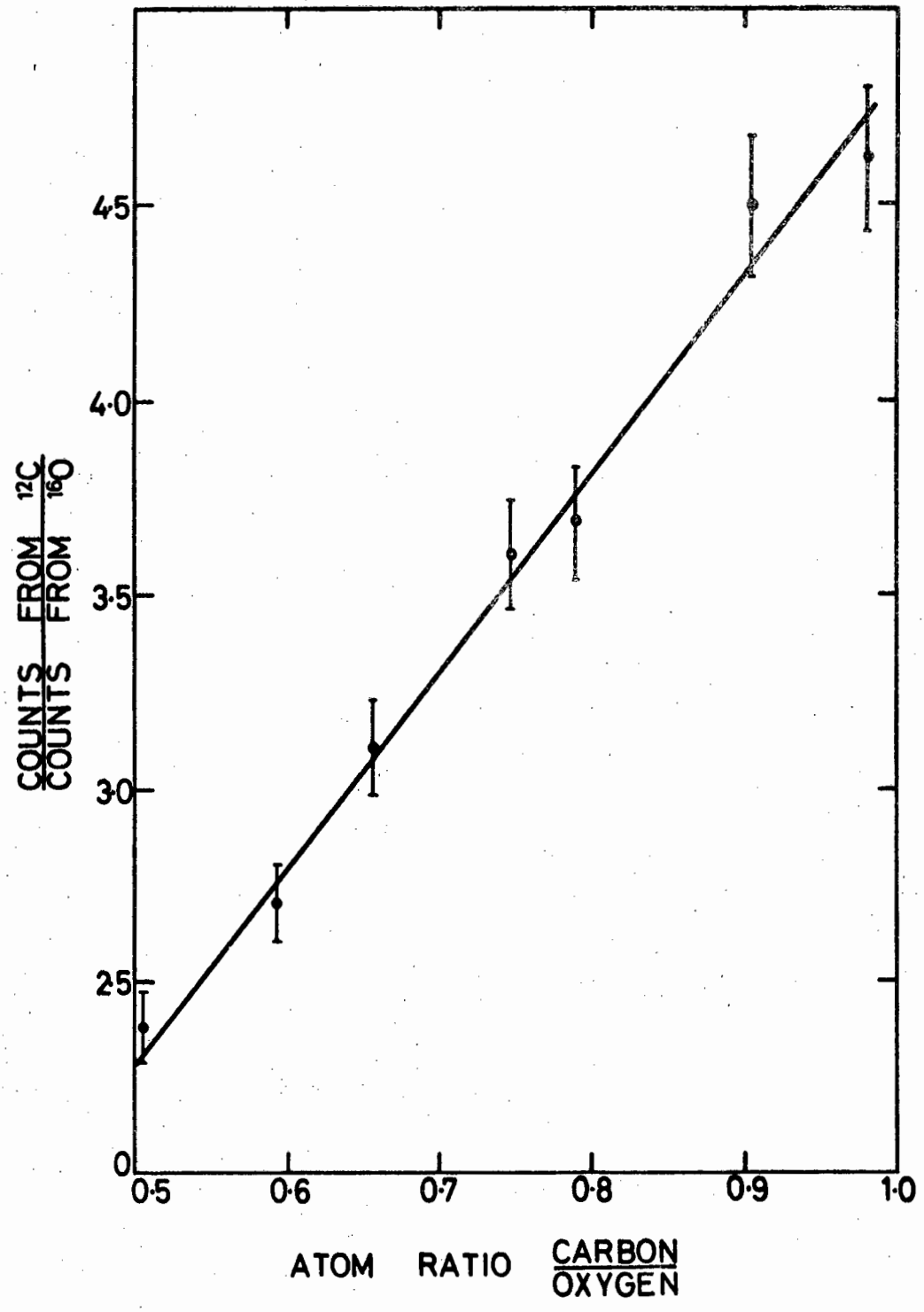


FIGURE 15. RESULTS OF $CO/CO_2$ ANALYSES

from equation 7 using the relative errors involved in the separate determinations of carbon and oxygen.

## PRECISION

From results given in the previous section it was found that over the range of sample compositions analysed the relative error was about $\pm$ 0.03. Since the method requires a measurement to be made of count rates, by observing events which are statistically random, the precision of an analysis will depend on the statistical errors involved in determining the count rate. When a gas sample of pressure, P, irradiated with a fixed total current, I, yields s counted events, and with the same current the background yields b events, the number of counts, c, obtained from the sample components is given by:

$$s = c + b = c_o.I.P + b_o.I \quad \ldots\ldots\ldots\ldots\ldots \quad (8)$$

where

$c_o = c/I.P$ = sample counts per unit current per unit pressure

and

$b_o = b/I$ = background counts per unit current.

The relative error, $\Delta R/R$, in determining the resultant count from the sample is given by:

$$\frac{\Delta R}{R} = \frac{\sqrt{c_o.I.P + 2.b_o.I}}{c_o.I.P} \quad \ldots\ldots\ldots\ldots\ldots \quad (9)$$

Using this relationship the gas pressure may be calculated for which the relative error does not exceed the experimental error of the method at the corresponding total current, $\underline{I}$. The minimum elemental concentration in the gas, for which the neutron count can be determined with a precision of $\pm$ 3.0%, has been calculated for carbon, nitrogen and oxygen. The values listed in Table X show that microgram quantities of these three elements can be determined without special precautions being taken to reduce the existing background. Clearly, if analyses are to be carried out at lower concentrations than those given in Table X the relative error of the result will be greater. It should be noted that the results in Table X were calculated for a maximum total current of 20 millicoulombs requiring an irradiation of about 3 hrs. When longer irradiation periods are practicable the minimum quantity of these elements, which can be determined without sacrificing precision, may be reduced.

## SENSITIVITY

The background count rates measured over the neutron energy regions corresponding to $n_0$ neutrons from carbon-12, nitrogen-14 and oxygen-16 were respectively 7733, 242 and 1170 counts per millicoulomb for a beam of 3 MeV deuterons. Using these values the minimum detectable amounts of the three nuclides can be deduced if it is assumed that the minimum

TABLE X

PRECISION LIMITS FOR ELEMENTAL ANALYSES

| Relative Precision % | Total Current milli-coulombs | Micrograms per $cm^2$ cross sectional area of beam | | |
|---|---|---|---|---|
| | | $^{12}C$ | $^{14}N$ | $^{16}O$ |
| ± 3.0% | 1 | 5.18 | 28.40 | 16.79 |
| | 2 | 3.46 | 16.67 | 10.75 |
| | 10 | 1.50 | 5.60 | 4.25 |
| | 20 | 1.06 | 3.67 | 2.92 |
| ± 10.0% | 1 | 1.42 | 5.29 | 3.99 |
| | 2 | 0.98 | 3.49 | 2.71 |
| | 10 | 0.44 | 1.43 | 1.18 |
| | 20 | 0.31 | 0.99 | 0.82 |

number of counts detectable from these nuclides should be three times greater than the relative standard deviation in the background count. The results of such calculations are given in Table XI for total currents of 1, 2, 10 and 20 millicoulombs requiring respectively irradiations of 10, 20, 100 and 200 minutes. These values represent the limiting sensitivity for qualitative detection of the elements in contrast to the limits for quantitative determination discussed previously.

Despite the comparatively high background in the energy region corresponding to neutrons from carbon, this element could be determined with greatest sensitivity because the $^{12}C(d,n_0)^{13}N$ reaction has a relatively high cross section. As the energies of their characteristic neutron groups were well resolved, the presence of both carbon and oxygen in the sample hardly reduced the sensitivity with which each could be determined. However, the presence of nitrogen in a sample affected the sensitivity with the other two elements could be determined. Nevertheless, carbon and oxygen could be determined in microgram quantities with a 2 millicoulomb total current, even when the nitrogen to carbon ratio was about 2500 : 1 by weight and the nitrogen to oxygen ratio was about 75 : 1.

TABLE XI

SENSITIVITY OF ELEMENTAL ANALYSES

| Total current millicoulombs | Micrograms per $cm.^2$ cross sectional area of beam | | |
|---|---|---|---|
| | $^{12}C$ | $^{14}N$ | $^{16}O$ |
| 1 | 0.29 | 0.90 | 0.77 |
| 2 | 0.21 | 0.63 | 0.54 |
| 10 | 0.09 | 0.28 | 0.24 |
| 20 | 0.06 | 0.20 | 0.17 |

## INTERFERENCES

When the sample contains other nuclides which yield neutrons with energies near to those of the neutron groups being used for analytical purposes, these nuclides would interfere with the precision of the analyses. Thus, during an elemental analysis with a deuteron beam, nitrogen-14 yields neutrons with energies close to those of the neutrons used to measure the carbon and oxygen content and hence, as mentioned above, reduces the precision with which these two elements can be determined.

Similar interference could be expected from gases containing enriched carbon-13, nitrogen-15 and oxygen-17 or 18. Figure 16 shows typical spectra obtained from the deuteron irradiation of carbon dioxide enriched in carbon-13 and of carbon dioxide enriched in oxygen-18 (peaks in the spectra corresponding to neutrons generated by nuclides other than carbon-13 and oxygen-18 are so labelled). It is clear that these two nuclides yield a relatively large number of neutron groups on irradiation with deuterons. The relative error introduced by interference from neutrons generated by the heavier isotopes would increase with increasing enrichment of these isotopes. Even in samples in which the heavy isotopes are not enriched, neutrons generated from them may still interfere with the determination of a minor component. For

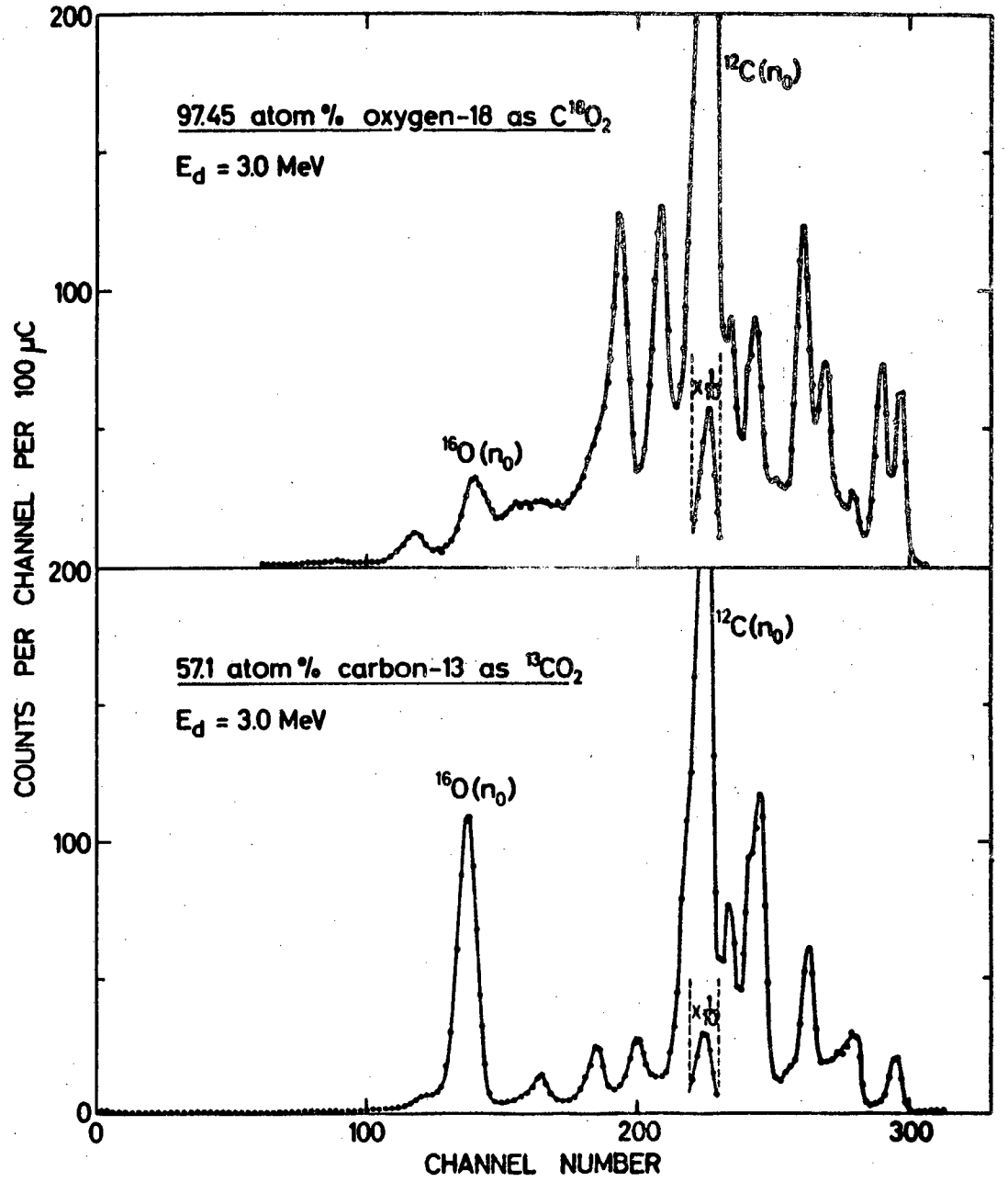


FIGURE 16. NEUTRON TIME-OF-FLIGHT SPECTRA OF $^{13}CO_2$ AND $^{18}CO_2$ GENERATED WITH 3.0 MeV DEUTERONS

$\theta = 30^{\circ}$
Flight path = 2.93 metres

example, a sample containing many carbon and only one nitrogen atom per molecule may contain carbon-13 in amounts comparable to the nitrogen content even though carbon-13 is not enriched.

# C H A P T E R  IV

# THE ISOTOPIC DETERMINATION OF THE HEAVIER ISOTOPES OF CARBON, NITROGEN AND OXYGEN

The measurement of neutrons from deuteron induced reactions on carbon-13, nitrogen-15, oxygen-17 and 18 is subject to interference from neutrons generated by the lighter isotopes. In addition Figure 16 illustrates that carbon-13 and oxygen-18 cannot be determined in the presence of one another by deuteron irradiation because the neutron groups they generate overlap in energy.

Reference to Table II shows that no neutrons can be generated from the very abundant nuclides carbon-12, nitrogen-14 and oxygen-16 by proton beams with energies of less than 5.931 MeV. Furthermore the values of the neutron energies listed in the table show that:

(i) Many neutron groups obtainable from oxygen-18 could be suitable for analytical purposes. Interference is not expected from the $n_0$ neutrons with energies close to those of the $n_3$ and $n_4$ neutrons from oxygen-18, and hence could be a possible source of interference.

(ii) Only one neutron group is produced by carbon-13. The group is singularly suited to measurement because it is not subject to interference by neutrons from any of the isotopes of oxygen or nitrogen.

(iii) Nitrogen-15 generates one neutron group, which has an energy comparable with the energy of neutrons generated by oxygen-17 and 18.

## NEUTRON SPECTRA

Typical neutron time-of-flight spectra obtained from enriched carbon-13 as $^{13}CO_2$, nitrogen-15 as $^{15}NH_3$ and oxygen-18 as $^{18}CO_2$ are shown in Figure 17. The energy of each neutron group in Figure 17 is about 150 keV lower than the corresponding values given in Table II. This is due to the energy lost by the proton beam in passing through the nickel window.

The spectrum obtained from oxygen-18 consisted of an isolated small single peak corresponding to the $n_0$ neutron group and a large composite peak which included counts from the neutron groups $n_1$, $n_2$, $n_3$ and $n_4$ that could not be resolved under the conditions of the experiment. For analytical purposes it is not necessary to resolve these neutron groups, because the relative number of counts obtained from each is determined by the cross section of each reaction which is constant at constant incident proton energy and a constant measuring angle. The small peak due to $n_5$ neutrons is just detectable, but because the detection efficiency for such low energy neutrons is much smaller than for neutrons of about 1 MeV or higher, the height of the peak is not a true reflection of the relative reaction cross section.

The $^{13}CO_2$ spectrum in the figure clearly shows that the $n_0$ neutrons were the only ones generated by this nuclide under the conditions of measurement. These neutrons can readily be distinguised from those of nitrogen-15 and oxygen-18 and can

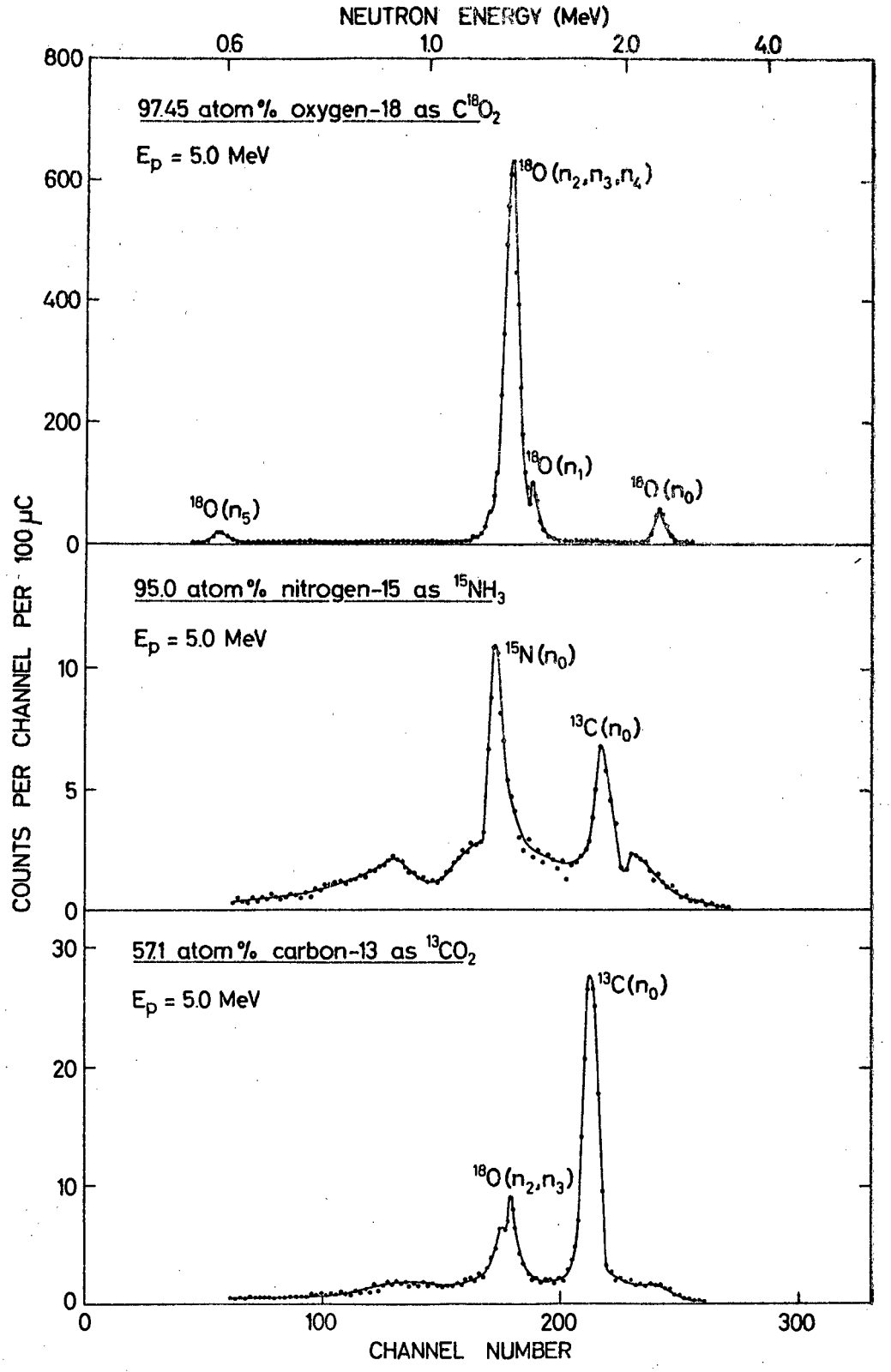


FIGURE 17. NEUTRON TIME-OF-FLIGHT SPECTRA OF $^{13}CO_2$ AND $^{18}CO_2$ GENERATED WITH 5.0 MeV DEUTERONS PROTONS

$\theta = 0^{\circ}$

Flight path = 3.13 metres

thus be used to provide a measure of the carbon-13 content.

The single neutron group from nitrogen-15 (see Figure 17) has an energy comparable with the energy of those neutrons from oxygen-18 produced in highest yield. The $^{15}NH_3$ spectrum also contains a peak corresponding to neutrons generated by carbon-13 but this peak is due to the background (vide infra). The relative neutron yield from the reaction $^{15}N(p,n_0)^{15}O$ is very low and the background count over the energy range of the $^{15}N(n_0)$ group is comparatively high (see Figure 18). For these reasons, the determination of nitrogen-15 was not studied in this investigation.

## BACKGROUND

A typical background spectrum as obtained from the irradiation of an empty gas cell with a beam of 5 MeV protons is given in Figure 18. This spectrum consists of two relatively prominent peaks corresponding to 1.752 and 1.328 MeV neutrons from carbon-13 and oxygen-18 respectively. These neutrons probably originate in deposits formed from residual vacuum oil vapours in the beam tube which decomposed at heated points of incidence of the irradiation beam. Reference to Figure 17 shows that the position of the background peak in the $^{15}NH_3$ spectrum is noticeably displaced towards an apparently higher energy compared with the corresponding peak in the $^{13}CO_2$ spectrum. The displacement indicates that the peak represents

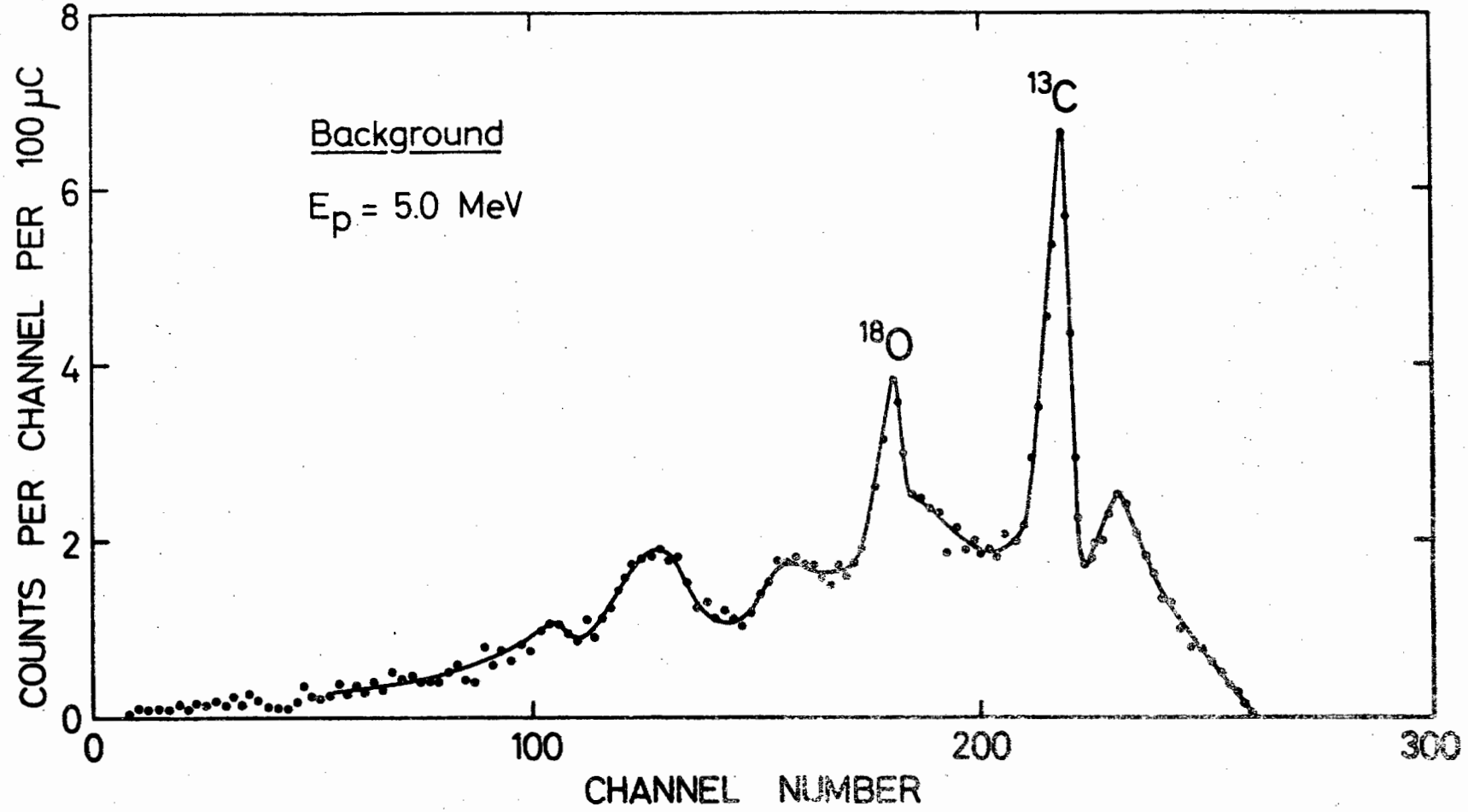


FIGURE 18. TYPICAL BACKGROUND SPECTRUM

$E_p$ = 5.0 MeV and $\theta = 0^\circ$
Flight path = 3.13 metres

neutrons from carbon-13 present in deposits somewhere between the cell and the pick-up probe in the beam tube. In addition there was a low continuum of counts (lower than that obtained from irradiation with 3 MeV deuterons) due to gamma-rays not entirely eliminated by pulse shape discrimination and neutrons scattered into the detector.

Unlike the case for deuteron irradiation where all nuclidic components of carbon, nitrogen or oxygen-containing gases generate neutrons at relatively low incident beam energies, proton irradiation at comparable energies does not generate neutrons in such large numbers because of the highly endoergic nature of the corresponding proton induced reactions on the more abundant lighter isotopes. Accordingly, the total number of neutrons produced in the gas cell from sources other than the nuclide under investigation, does not vary appreciably with the composition of the gas unless the gas contains other enriched isotopes of carbon, nitrogen or oxygen. Hence, the magnitude and spectral distribution of the background can be considered to be independent of the pressure and composition of the gas under analysis.

## CALIBRATION

The $n_0$ neutrons from oxygen-18 are readily resolvable from all other neutron groups that can be generated in gases containing only carbon, nitrogen and oxygen and would

therefore appear to be most suitable for analytical purposes. However, the neutron yield from the $(p,n_0)$ reaction induced by 5 MeV protons is so much lower than the yield from the combined $(p,n_i)$ reactions with i = 1, 2, 3 and 4, that the integrated neutron count over the energy region covered by this combined group provides a better index of the oxygen-18 content of the gas. With 5 MeV protons the appropriate energy region for integration lies between about 1.0 and 1.58 MeV. The integrated count in this region was used as a measure of the oxygen-18 content despite the fact that neutrons from nitrogen-15 and oxygen-17 might add to the total count.

As the neutron count is proportional to the number of target nuclei in the path of the beam, it was possible to utilize the integrated neutron count obtained from a single gas sample, but measured over a range of pressures, as a calibration curve. Calibration with a 5 MeV proton beam and approximately 10 atom per cent oxygen-18 as $^{18}CO_2$ over pressures ranging from 0.7 to 63.3 mm. Hg. and 57 atom per cent carbon-13 as $^{13}CO_2$ over pressures ranging from 0.5 to 12.0 mm. gave linear calibration curves with slopes respectively of 1080 and 87 counts per microgram per cm.$^2$ cross sectional area of the beam for a total current of 1 millicoulomb. These values show that the total effective cross section for the reactions $^{18}O(p,n_i)^{18}F$, with i = 1, 2, 3 and 4, was about nine times the cross section for the reaction $^{13}C(p,n_0)^{13}N$ under the

conditions of measurement.

## RESULTS OF ANALYSES

Table XII lists the results of some determinations of oxygen-18 in oxygen gas and in the presence of natural carbon dioxide and natural nitrogen with a proton beam of 5.0 MeV. The mean neutron count was 1095 counts per microgram per cm.$^2$ per millicoulomb which agrees with the calibration value, quoted above, within the precision of the method. The mean error of + 0.058 ngm. per cm.$^2$ provides a measure of the accuracy of the method and shows that there is no bias. The relative standard deviation was $\pm$ 3.38%.

The results of determinations of carbon-13 in carbon dioxide in the presence of natural nitrogen are given in Figure 19. The relatively large statistical errors shown in the figure were due to the low yield for the reaction $^{13}C(p,n_0)^{13}N$ and the comparatively high number of background neutrons with an energy similar to that of the neutrons used for analysis.

## PRECISION AND SENSITIVITY

The minimum weight of oxygen-18 for which the neutron count could be determined with a precision of $\pm$ 3.0% by irradiating with a total current of 1 millicoulomb, was found from equation 9 to be 1.76 µgm per cm.$^2$ oxygen-18. By

TABLE XII

SOME DETERMINATIONS OF OXYGEN-18 IN $O_2$, $CO_2$ and $N_2$ ?

$E_p$ = 5.0 MeV  $\theta = 0^o$

| Sample number | Gas | µgm. $^{18}O$ per cm.$^2$ beam area | | Error | Relative error | Neutron counts per 1000 µC | Neutron counts per 1000 µC per µgm. per cm.$^2$ beam area |
|---|---|---|---|---|---|---|---|
| | | Known A | Found B | (B-A) | 100(B-A) /A | N | N/A |
| 23 | $O_2$ | 2.470 | 2.209 | - 0.261 | -10.593 | 2617 | 1060 |
| 39 | $O_2$ | 4.438 | 4.081 | - 0.357 | - 8.046 | 4639 | 1045 |
| 42 | $O_2$ | 9.950 | 9.712 | - 0.238 | - 2.396 | 10720 | 1077 |
| 40 | $O_2$ | 15.093 | 15.142 | + 0.049 | + 0.327 | 16584 | 1099 |
| 15 | $O_2$ | 20.687 | 21.398 | + 0.711 | + 3.435 | 23340 | 1128 |
| 26 | $N_2$ | 3.322 | 3.077 | - 0.245 | - 7.387 | 3555 | 1070 |
| 20 | $N_2$ | 6.846 | 6.885 | + 0.039 | + 0.569 | 7667 | 1120 |
| 43 | $N_2$ | 12.082 | 12.193 | + 0.111 | + 0.915 | 13399 | 1109 |
| 18 | $N_2$ | 19.657 | 19.443 | - 0.214 | - 1.089 | 21228 | 1080 |
| 19 | $N_2$ | 27.358 | 26.721 | - 0.637 | - 2.330 | 29088 | 1063 |
| 28 | $N_2$ | 31.462 | 32.512 | + 1.050 | + 3.336 | 35342 | 1123 |
| 22 | $CO_2$ | 3.876 | 3.662 | - 0.214 | - 5.521 | 4187 | 1080 |
| 37 | $CO_2$ | 5.697 | 5.632 | - 0.065 | - 1.143 | 6314 | 1108 |
| 16 | $CO_2$ | 10.627 | 11.562 | + 0.935 | + 8.794 | 12718 | 1197 |
| 25 | $CO_2$ | 17.714 | 18.232 | + 0.518 | + 2.922 | 19921 | 1125 |
| 41 | $CO_2$ | 24.542 | 24.348 | - 0.194 | - 7.890 | 26526 | 1081 |
| 17 | $CO_2$ | 36.834 | 35.847 | - 0.987 | - 2.678 | 38944 | 1057 |

Mean Error = + 0.058 ngm. per cm.$^2$ beam area

Mean neutron count per µgm. $^{18}O$ per cm.$^2$ beam area per millicoulomb = 1095

Relative standard deviation = $\pm$ 3.38%

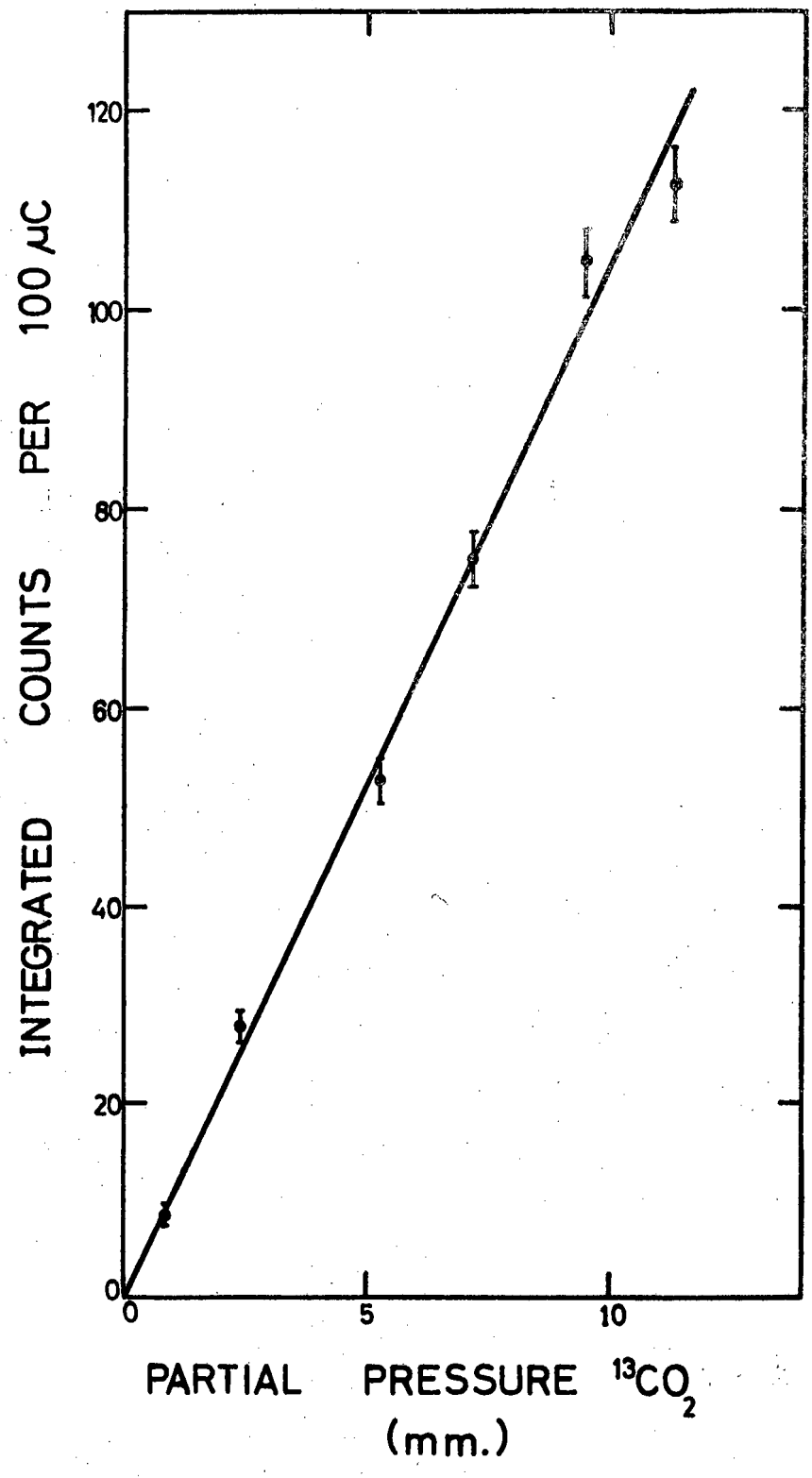


FIGURE 19. RESULTS OF $^{13}C$ ANALYSES

increasing the total current to 20 millicoulombs, about 280 ngm per cm.$^2$ of oxygen-18 could be measured with the same precision. When a lower precision of $\pm$ 10% was acceptable, this limit was reduced to 80 ngm per cm.$^2$ Despite the low effective cross section of the $^{12}C(p,n_0)^{13}N$ reaction, an irradiation with 20 millicoulombs total current could be used to analyse about 940 ngm per cm.$^2$ quantities of carbon-13 with a precision of $\pm$ 10%.

The background over the energy range of the $n_1$, $n_2$, $n_3$ and $n_4$ neutrons from oxygen-18 amounted to 706 counts per millicoulomb. Under these conditions the sensitivity limit for the detection of oxygen-18 with 1 millicoulomb total current was 72 ngm per cm.$^2$ By increasing the total current to 20 millicoulombs it should be possible to detect as little as 16 ngm. of oxygen-18 per cm.$^2$ This is equivalent to detecting the presence of oxygen-18 in natural oxygen in a gas cell 3 cm. long filled to a pressure of 1 mm.

## INTERFERENCES

When the determination has to be carried out in the presence of oxygen in which the oxygen-17 concentration is not enriched interference from this nuclide is unlikely. However, it frequently happens that preparations enriched in oxygen-18 are also enriched in oxygen-17 albeit to a smaller extent. In such cases interference from oxygen-17 is likely and the extent

of this interference remains to be studied.

In the presence of carbon, oxygen-18 can readily be determined because none of the stable isotopes of this element can produce interfering neutrons. In the presence of nitrogen interference from neutrons generated by nitrogen-15 may be expected when the concentration by weight of nitrogen-15 is seven times that of oxygen-18. At the isotopic concentrations of oxygen-18 and nitrogen-15 found in nature, neutrons from nitrogen-15 would introduce significant errors into the determination of oxygen-18 when the nitrogen to oxygen atom ratio is greater than about 4 : 1.

Other elements from which interference is energetically possible, when 5 MeV protons are used, are neon (from $^{22}Ne$) and sulphur (from $^{36}S$). The presence of neon in samples containing enriched oxygen-18 is improbable. Sulphur-36 occurs in nature in an isotopic concentration of 0.014 atom per cent. Interference from this nuclide is thus expected to be small in unenriched samples, but the extent of the interference remains to be studied.

# C H A P T E R  V

# ATTEMPTS AT ANALYSING VOLATILE ORGANIC COMPOUNDS

The separate determination of carbon, nitrogen and oxygen in the gaseous phase by means of time-of-flight spectrometry on the neutrons generated by deuteron-induced reactions, suggested that the method had great potential use for the analysis of volatile organic compounds. However, the extension of the technique to organic vapours was found to be closely connected with the limitations of the method.

## INTERFERENCES AND LIMITATIONS

### FROM SAMPLE COMPONENTS

The type of interference which could be expected has already been discussed in Chapter III. Because most organic molecules contain relatively few nitrogen atoms relative to the number of carbon and oxygen atoms, little interference in the determination of the latter two elements would be caused by the presence of nitrogen. However, the measurement of the nitrogen content of most samples would require irradiation with a comparatively low energy deuteron beam to permit measurement in the absence of neutrons from carbon-12 and oxygen-16, which, at the higher deuteron energy, could contribute to the background continuum in the energy region corresponding to the $n_0$ neutrons from nitrogen-14. Interference from the heavier isotopes could not be eliminated in the same way and the determination of nitrogen in an organic sample containing many

carbon and only one nitrogen atom per molecule would be affected by the comparatively high carbon-13 content.

FROM HEATING THE SAMPLE

Local heating of the gas in the path of the beam could decrease the density of the gas and cause a decreased rate of neutron production. This effect was, however, not observed at the low average current densities used in this investigation

FROM HEATING THE CONTAINER

On passing through the nickel window into the cell, a fraction of the energy of the irradiating beam is dissipated as local heating on the window. At the tantalum backing the beam is entirely stopped causing a very high temperature over a small area of the metal. The high temperature at these two hot spots would severely restrict the usefulness of the method if the gas sample under analysis contained a component which decomposed to non-volatile products at the temperatures concerned. The non-volatile products would tend to deposit in the path of the beam and become a source of neutrons. The background would then become overwhelming and make accurate analyses difficult. Moreover the cell would be rendered unusable for subsequent analyses.

As an example of thermal decomposition, the irradiation of acetonitrile vapours may be cited. A sample of liquid $CH_3CN$ was connected directly to the irradiation cell to build up the

saturation vapour pressure. During irradiation it was observed that the neutron count from the sample increased rapidly. The resultant time-of-flight spectrum given in Figure 20 is dominated by the peak corresponding to neutrons from carbon-12. By contrast the peaks generated by the neutrons from nitrogen-14 are scarcely discernible. The peak caused by carbon in the spectrum is noticeably displaced to an apparently lower energy, compared with the position of the corresponding peak obtained with methane (shown by an arrow in Figure 20). The apparent energy displacement of the peak was due to the fact that the carbon-12 neutrons from acetonitrile were mostly generated at the backing whereas those from methane were generated about the middle of the cell. Examination of the cell after irradiation revealed a carbon deposit on the inside of the nickel window and a thick tarry residue on the backing. Clearly the amount of decomposition products on the backing would have been considerably lower, had the cell been isolated from the liquid during the irradiation.

## APPLICATION TO ORGANIC VAPOURS

If the method is to be of use in the analysis of thermally unstable organic vapours, either decomposition must be prevented or the deleterious effects of decomposition must be minimised.

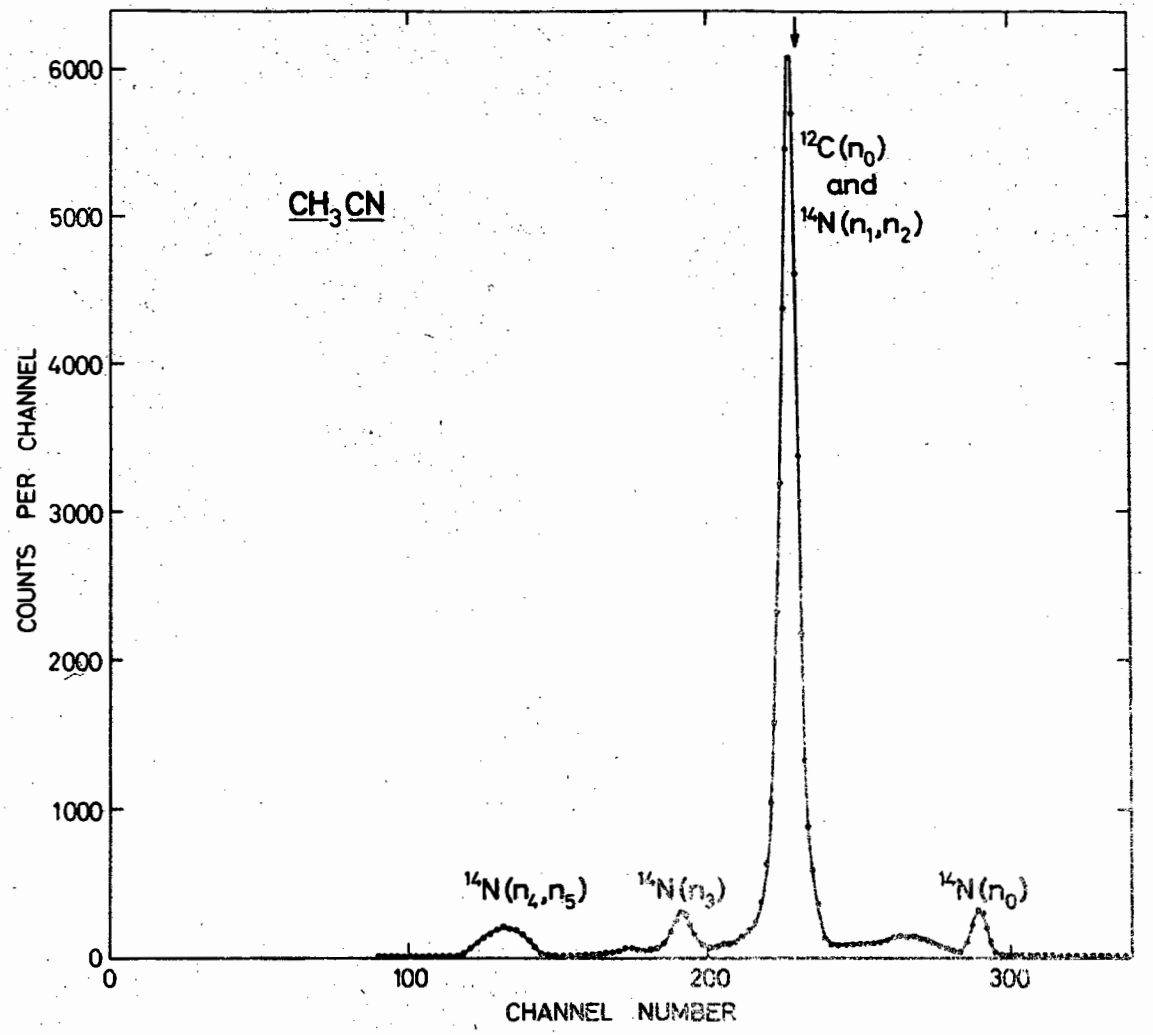


FIGURE 20. NEUTRON TIME-OF-FLIGHT SPECTRUM OF $CH_3CN$

$E_d$ = 3.0 MeV

$\theta$ = 30°

Flight path = 2.94 metres

PREVENTION OF DECOMPOSITION

A possible approach would be the use of materials with better heat conducting properties in the construction of the cell, and the use of some cooling device. Such an approach is, however, unlikely to solve the problem since the heating effect generates a temperature of nearly 1000°C and is very localised. Also, any cooling system would have to make contact with the nickel window and yet not result in energy degredation of the deuteron beam.

A second approach would be to decrease the heating effect of the beam by decreasing the average beam current, but the neutron count rate would then drop and hence the time required for an analysis would have to be increased. Attempts to increase the neutron count rate could then be made by increasing the length of the irradiation cell, or by increasing the cross sectional area of the beam. However, an increase in the cell length would increase the uncertainty in the flight path of the neutron, resulting in a broadening of the spectral peaks. Changes in the cross section of the beam are limited to the maximum cross sectional area obtainable from the accelerator.

UTILISATION OF DECOMPOSITION

An entirely different approach involves decomposition of the sample under controlled conditions. Non-volatile decomposition products may then be deposited over a selected area and subsequently removed from the path of the beam to make analyses

of the volatile materials possible. This procedure transforms the analysis into a four stage process and necessitates the construction of a different irradiation cell shown in Figure 21.

Firstly, the cell and its measured contents are irradiated for a short period with an unpulsed beam of deuterons at a high current (8-12 microamp.) in the position I shown in Figure 22. During this operation the high temperature generated at the tantalum backing could cause decomposition of most organic vapours and the deposition of non-volatile materials at the hot spot. The tantalum backing is 0.25 mm. thick, sufficient to stop the beam entirely, and its thermal conductivity appeared to be suitable to ensure localisation of the deposit. The flanged adapter (see Figure 22) is used to move the point of incidence of the beam on the backing to a markedly off-centre position. The dimensions of the dummy cell were chosen such that the deposit could be placed in the path of the beam during a subsequent irradiation.

Secondly, the cell without its dummy is mounted in position II as shown in Figure 22 with the nickel window end attached to the adapter and any deposit on the tantalum backing in the path of the beam. A second irradiation is carried out with a pulsed deuteron beam of a cross sectional area large enough to cover the entire deposit. The time-of-flight spectrum recorded at this stage would represent neutrons emitted from the deposit and from any volatile material in the cell, and

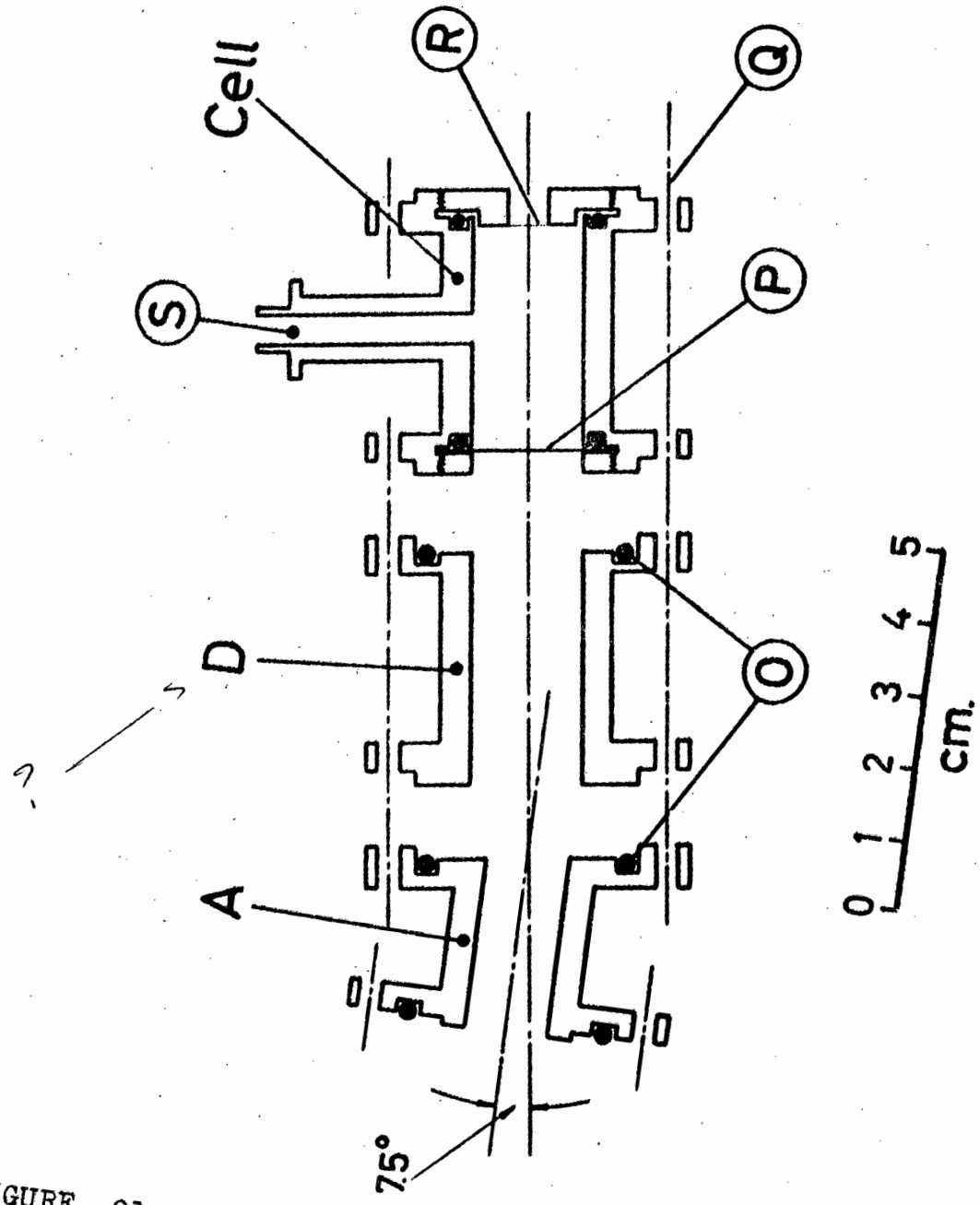


FIGURE 21. IRRADIATION CELL ASSEMBLY FOR DECOMPOSING AND ANALYSING ORGANIC VAPOURS

A : Flanged adapter
B : Dummy cell
O : Vacuum O-rings
P : Tantalum back of cell
Q : Centre line for assembly screws
R : Nickel window
S : Connection for vacuum apparatus

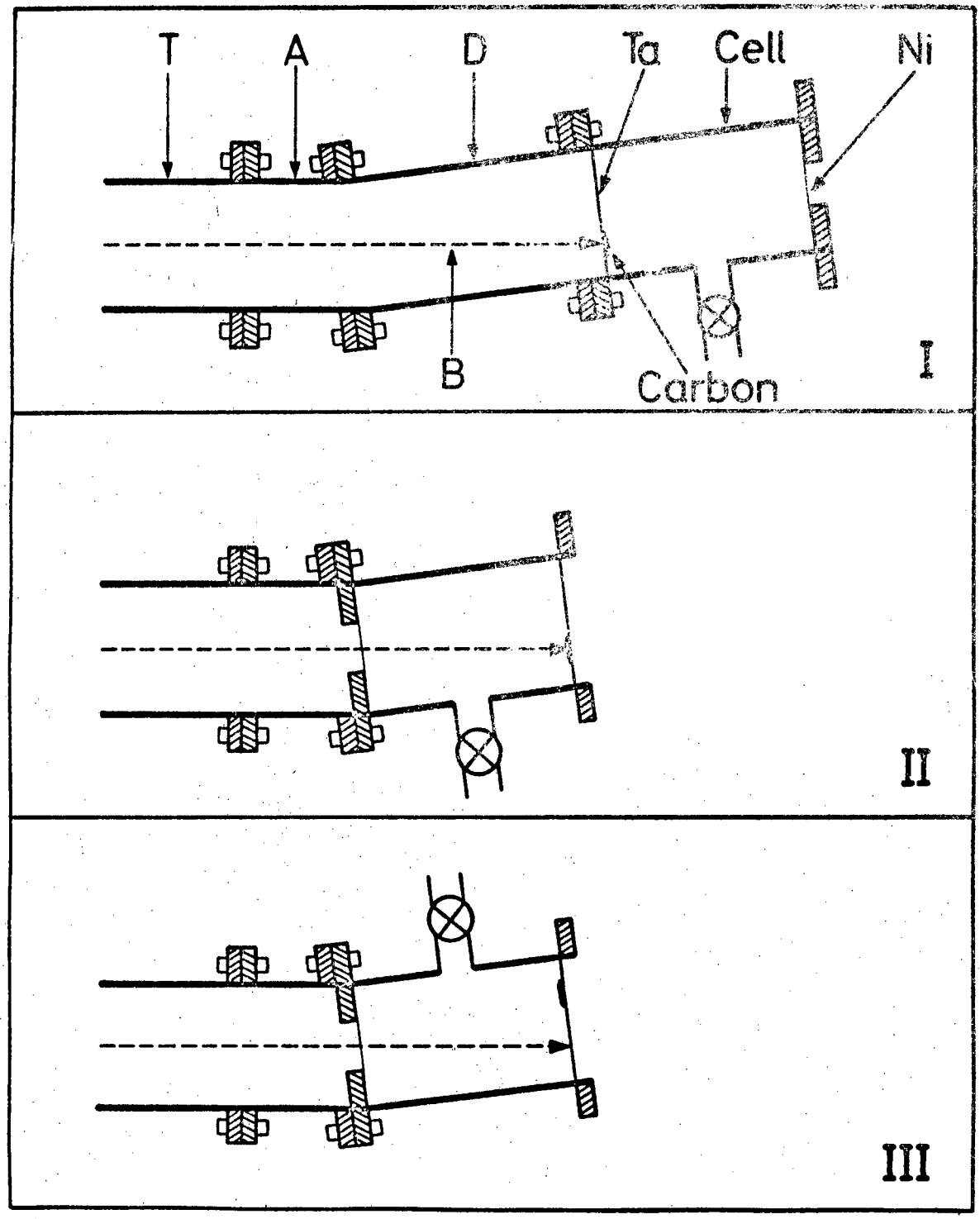


FIGURE 22. ANALYTICAL IRRADIATION SEQUENCE

I : Preliminary decomposition
A : Flanged adapter
B : Path of irradiating beam
C : Dummy cell

II : Analysis of carbon deposit

III : Analysis of residual gas phase and background

? → D ?

the background.

Thirdly, the cell is rotated through 180° about its length (position III, Figure 22). Because the deposit would not be in the centre of the tantalum backing, the rotation of the cell would effectively remove the deposit from the path of the beam. The time-of-flight spectrum recorded during this irradiation would represent neutrons emitted from the volatile material and the background.

Fourthly, the cell is evacuated and a spectrum representing the background can be obtained.

From the data obtained at the second, third and fourth irradiation, the required analytical results may be computed.

## RESULTS AND DISCUSSION

The area on the tantalum backing immediately surrounding the point of incidence of the direct beam used in stage I (see Figure 22) of the analytical procedure outlined above, will be referred to in this discussion as the "stage I" position and the area of the backing irradiated in stages III and IV will be called the "stage III" position.

The decomposition step, stage I of the procedure, was tested on the vapours of acetonitrile, acrylonitrile, acetone, benzene, methanol and ethanol. In all cases, after irradiation with a direct beam of high current for about ten minutes, examination of the cell showed a localised black deposit in

the off-centre position on the tantalum backing at the point of incidence of the direct current beam. A similar irradiation carried out on an empty cell caused no visible change on the tantalum backing. These results suggested that any deposit formed on the backing during the stage I irradiation with a direct beam owed its origin to the sample under analysis. The thermal properties of tantalum thus appeared adequate to ensure localisation of any deposit which formed.

On completion of these preliminary tests, an attempt was made to apply the complete analytical procedure to the vapours of methanol and ethanol. The deposit in the "stage I" position was expected to generate a time-of-flight spectrum dominated by a large peak corresponding to neutrons from carbon-12, whereas the gaseous phase in the cell was expected to show a spectrum characterised by two smaller peaks generated by the carbon and oxygen of volatile decomposition products.

The resolved spectra obtained from the irradiations are given in Figure 23. The spectra corresponding to the "stage I" deposits indicate the presence of carbon in smaller quantity then expected and the totally unexpected presence of oxygen. The gaseous phase produced neutron groups which conformed with those predicted although the number of neutrons from carbon-12 was much greater than anticipated. The background spectra from both the methanol and ethanol cells contain a substantial neutron peak from carbon-12 indicating the presence of a

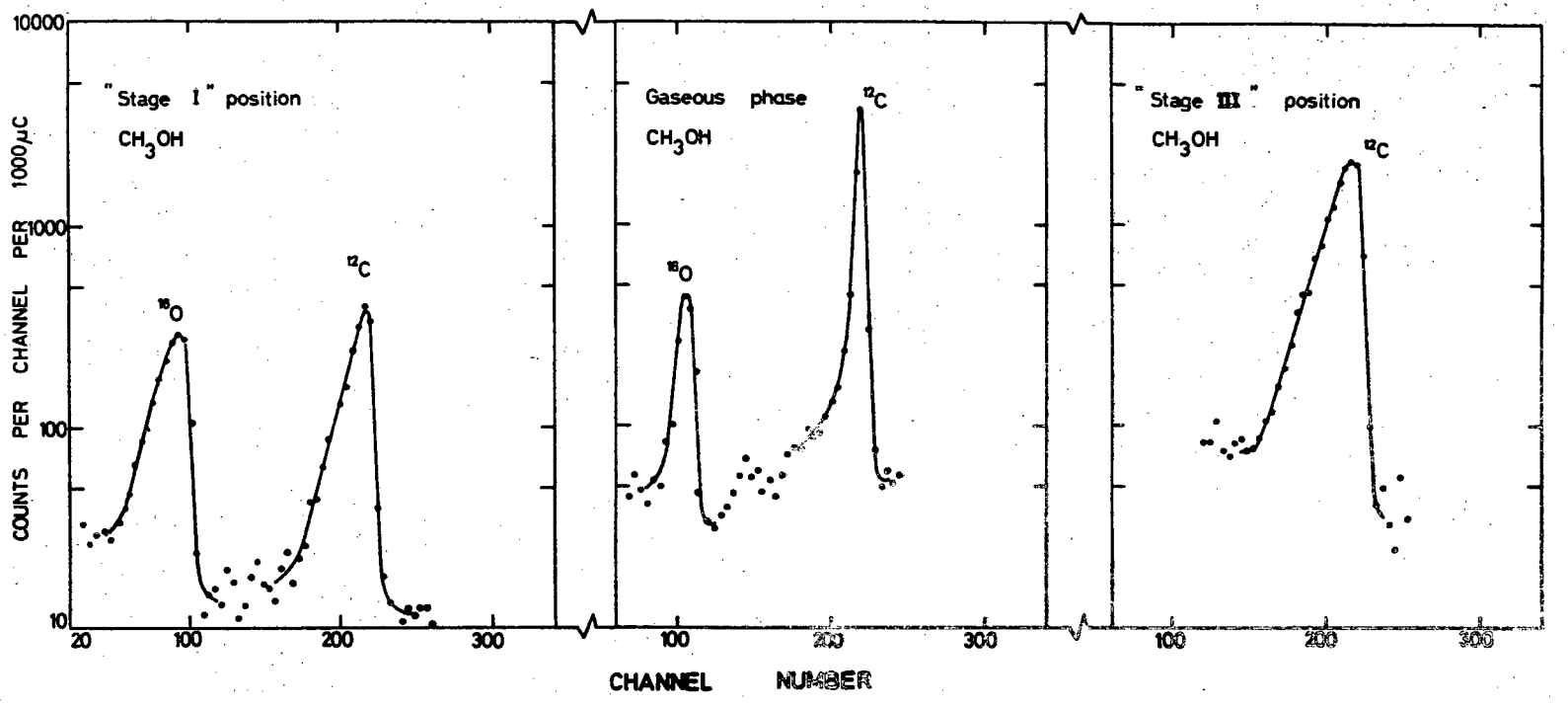


FIGURE 23(a). TIME-OF-FLIGHT SPECTRA FROM THE ANALYSIS OF $CH_3OH$

$E_d$ = 3.0 MeV

$\theta$ = $30^\circ$

Flight path = 2.93 metres

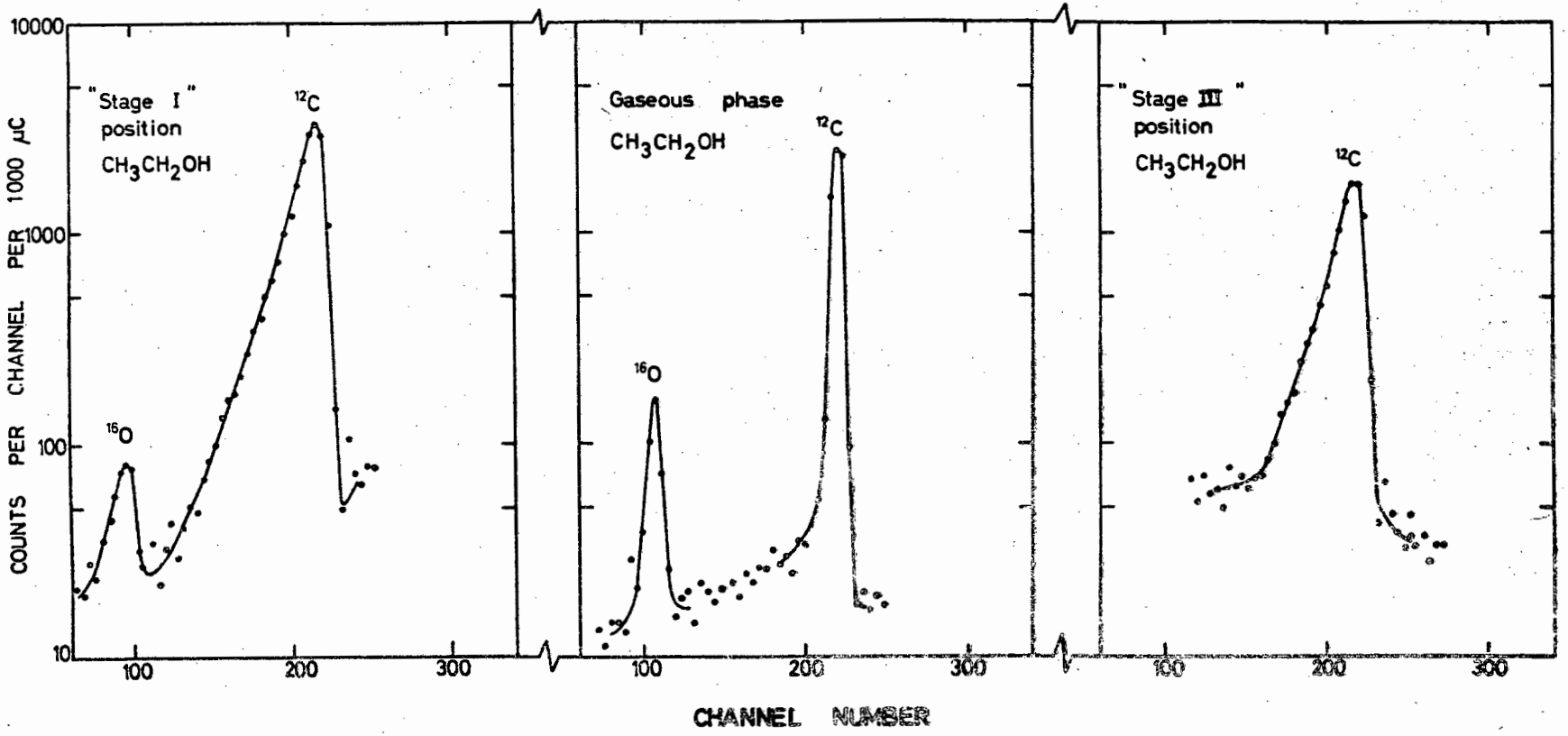


FIGURE 23(b). TIME-OF-FLIGHT SPECTRA FROM THE ANALYSIS OF $CH_3CH_2OH$

$E_d$ = 3.0 MeV

$\theta$ = 30°

Flight path = 2.93 metres

significant carbon deposit on the tantalum backings in the "stage III" positions, even though examination of the cells did not reveal any visible material in the "stage III" positions.

Symmetrical peaks represent neutrons generated in the gaseous phase whereas neutrons generated in the deposit gave rise to a peak tailing on its low energy side, indicative of neutrons generated at a point beneath the surface of the deposit. The difference in energy between such neutrons and those produced at the surface represents the energy lost by the irradiating beam in traversing target material before arriving at the point of reaction. Consequently, this energy loss can be used to provide a qualitative indication of the thickness of the deposit or alternately the depth to which atoms of the deposited material have penetrated the metal lattice of the tantalum backing. In the case of ethanol, the energy loss calculated (17) from the spectra was found to be 50 keV. If this value is used as a measure of the depth to which carbon has diffused into tantalum, a maximum depth of 60 μ is obtained.

The ratio of oxygen in the "stage I" deposit to oxygen in the gaseous phase was approximately the same for both methanol and ethanol. An oxygen balance, obtained by integrating the number of neutron counts under the appropiate peaks, indicated that 99.6 per cent of the known oxygen content in the methanol cell could be accounted for but only 66.5 per cent in the ethanol cell. Because the distribution of any carbon

deposited over the area of the backing not irradiated, is unknown, it was impossible to calculate a carbon balance for the samples. However, the ratio of carbon to oxygen in the gaseous phase could be determined and was found to be 0.7 : 1 for methanol and 1.3 : 1 for ethanol.

Interpretation of the results was facilitated by taking into consideration the relevant high temperature chemistry of tantalum (18): $Ta_2O_5$ may be formed by heating tantalum metal in the presence of oxygen and $TaO_2$ by reduction of the pentaoxide with carbon. Tantalum carbide (which has an interstitial structure, the carbon atoms occupying octahedral holes in the close packed arrays of metal atoms) may be formed by direct union of the elements at high temperature, by heating the metal in the vapour of a suitable hydrocarbon or by reduction of the oxides with carbon.

From these data several posible explanations of the observed spectra may be proposed: Firstly, the hot tantalum spot could act as a catalyst in the cracking of organic molecules resulting in the possible formation of free radicals and other transient species. These could react further with molecules of the original gas to form non-volatile products which may deposit on any surface. If this occurred, carbon could be found in the "stage III" position. Secondly, whilst the heating effect is very intense at the point of incidence, the direct current beam is used long

enough for the tantalum backing as a whole to become heated by conduction and hence to cause deposition of non-volatile material over its entire surface. If this were the case, carbon could again be found in the "stage III" position. Thirdly the tantalum may react chemically with the sample gas to form oxides, carbides or other metal compounds depending on the elemental composition of the sample. This would explain the presence of carbon and oxygen and also the blackening of the tantalum in the "stage I" position because the oxide, $TaO_2$, and the carbide, TaC, are black. Fourthly, the pyrolysis of the organic compound at the hot tantalum surface could result in the formation of carbon monoxide, carbon dioxide and other thermally stable gases containing carbon. This explains the observation of the presence of carbon and oxygen in the gaseous phase and could account for the unexpectedly high carbon content.

Some or all of these explanations may be valid whilst other explanations may become evident after further study. The essential feature of this approach to the analysis of thermally unstable samples is the deposition of the most highly concentrated element (which is carbon in the case of organic compounds) over a selected localised area of the backing and its subsequent removal from the path of the beam to permit the determination of the less concentrated elements. Further development of the method will require the cell to

be redesigned to ensure the complete localisation of the heating effect of the beam and the use of a backing material which will promote the preferential deposition of carbon from organic compounds. An elucidation of the exact nature of the black deposit on the tantalum backing will only be possible after a thorough analysis of the surface layers of the backing.

# SUMMARY

A novel method, utilizing time-of-flight spectrometry on neutrons emitted by reactions induced with pulsed deuteron and proton beams, is described for the elemental and isotopic determination of carbon, nitrogen and oxygen in the gaseous phase.

The three elements were determined in thermally stable gas samples by measuring the neutrons emitted from (d,n) reactions induced by a pulsed deuteron beam of 3.0 MeV. Pulses were of 5 nsec. duration and 400 nsec. apart. The number of neutrons of each energy varied linearly with the partial pressure of the gas under investigation, provided the energy loss of the irradiating beam in the gas sample was negligible. When gas target pressures exceeded about 50 mm., the energy lost by the beam was significant and caused a deviation from linearity in the oxygen calibration curve, but the linear relationship could be restored when correction was made, for the change in the relative efficiency of neutron detection, and from the effective excitation curve for the reaction $^{16}O(d,n_0)^{17}F$.

Methane, nitrogen and oxygen and mixtures of $CO_2/N_2$ and $CO_2/CO$ were analysed at gas target pressures ranging from 1 to 100 mm. The relative standard deviation of the method was about $\pm$ 3% for the determination of all three elements. The average time required for an irradiation was about 10 minutes

which corresponded to a total current of 1 millicoulomb. Under these conditions 5.18, 28.40 and 16.79 μgm. per cm.$^2$ beam area respectively of carbon, nitrogen and oxygen could be determined within the precision of the method. The method is sufficiently sensitive to enable the qualitative detection of carbon, nitrogen and oxygen in amounts of 0.06, 0.20 and 0.17 μgm per cm.$^2$ respectively, if a total current of 20 millicoulombs is used.

Oxygen-18 and carbon-13 were determined in gas mixtures containing natural carbon, nitrogen and oxygen, by using neutrons emitted from (p,n) reactions induced by a pulsed proton beam of 5.0 MeV. The variation in the integrated neutron count from the neutron energy groups studied, was directly proportional to the weight of the target nuclide in the path of the beam. Because the neutron yield from the reactions $^{18}O(p,n)^{18}F$ was comparatively high and the effective cross section for the reaction $^{13}C(p,n)^{13}N$ comparatively low, oxygen-18 could be determined with much greater sensitivity than carbon-13. Quantities of 1.76 μgm per cm.$^2$ of oxygen-18 could be determined with a precision of $\pm$ 3%, by irradiating with a total current of 1 millicoulomb. When the total current was increased to 20 millicoulombs it was possible to detect 16 ngm per cm.$^2$ of oxygen-18.

All analyses of thermally stable gases were non-destructive and could be carried out in situ.

The vapours of most organic compounds could not be analysed in the gas irradiation cell because the high temperatures generated by the beam at the cell window caused decomposition of the sample. Non-volatile decomposition products, deposited on the cell window in the path of the beam, led to comparatively high neutron yields from carbon-12 and made the cell unusable for subsequent analyses. A different analytical procedure was tried in which decomposition of the sample under analysis was controlled and non-volatile products deposited over a selected localised area of the rear cell wall. The deposit could, subsequently, be removed from the path of the beam to permit the measurement of gaseous decomposition products. Application of this procedure to the analysis of the vapours of methanol and ethanol showed that the method had potential, but more development was needed.